RAL-TR-2002-007

A General Model for the Gain of Gas Avalanche Counters

J.E. Bateman

Instrumentation Department, Rutherford Appleton Laboratory,
Chilton, Didcot, Oxon, OX11 0QX, UK

9 April 2002

Abstract

A simple, general model of the avalanche process in gas counters is described. Applicable to all the common forms of gas avalanche detector – wire, microstrip, point anode and parallel gap, the model describes the gain process in terms of two pseudo-physical constants which are effectively invariant over the working range of any given detector configuration. For counter operation over a wide range of conditions (e.g. very different gas pressures) the model is extended so that four parameters are required to model the gain. Applications of the model to the characterisation, operation and design of a variety of counter types are given.

1. Introduction

Since their invention in the early twentieth century gas counters have proved extremely adaptable as detectors of ionising radiation, not only on account of the ease with which the detecting medium may be changed (e.g. ^{3}He for slow neutrons or xenon for hard x-rays), but also due to the geometric flexibility of the sensitive volume and the avalanche region. Thus planar (parallel gap) [1], linear (wire) [2] or point (needle) [3] detectors have all been successfully used in a wide range of applications, some with imaging capability and some without. Recent technological advances associated with the electronics industry such as micro-lithography and precision printed circuit manufacture have revolutionised one's ability to fabricate the small electrode structures required in many designs. The three geometries as implemented by this new technology are exhibited in the Compteur a Trous (CAT) [4], the Gas Microstrip Detector (GMSD) [5] and the MicroDot Detector (MDD) [6].

In the absence of a general model of the avalanche process, design and operation of the devices is largely empirical. There is an extensive literature with models for the gain of the standard single wire proportional counter [7-16], which however, in general exhibit little practical utility for the design and operation of gas counters. This report elaborates a simple model of the avalanche gain process which is applicable to all detector geometries and which allows the behaviour of the gas gain to be explored as a function of the geometry and the thermodynamic gas variables pressure (P) and temperature (T). This provides useful assistance in the design, characterisation and operation of the new families of gas avalanche detectors.

2. The Gain Model

In an electron avalanche process the controlling parameter is the specific ionisation (α), the number of ion pairs being generated per unit length at any given point in the high field region in which the amplification is occurring. In gases α is generally known as the Townsend Coefficient. The total multiplication or gas gain (M) achieved by an electron in the transit from cathode to anode is given by:

$$\ln M = -\int_{r_a}^{r_c} \alpha dr \qquad (1)$$

where the integral is performed along the electron path from the cathode to the anode.

An electron drifting in a high electric field can acquire enough energy in the free path between atomic interactions to (at lower field values) excite the gas atoms and (as the field increases) ionise them, so contributing to the specific ionisation α. The excitation processes absorb electron kinetic energy and so keep α low (although in binary gas mixtures excited atoms can generate ionisation by secondary interactions such as Penning processes and photo-ionisation by fluorescent photons). The simplest model for α neglects these effects and considers only the collision ionisation process in which an energetic electron directly ionises a gas atom. This is characterised by the parameters - W the threshold energy for ionisation (the outer-most atomic electron binding energy) and σ the cross-section for the ionisation process. Any electron of the population (which is assumed to have a Maxwellian energy distribution) with a

kinetic energy above this value is assumed to cause an ionisation event. This leads to the following expression for α [17] :

$$\alpha = \frac{1}{\lambda}\exp\left(\frac{-W}{E\lambda}\right) \qquad (2)$$

where λ is the electron mean free path and E is the local electric field strength. If σ is the effective cross-section for the ionisation process we can write :

$$\lambda = \frac{1}{N_L \sigma} \qquad (3)$$

where N_L is Loschmidt's Number, the number of atoms (molecules) per unit volume. In turn the gas laws yield the relation :

$$N_L = \frac{N_A P}{RT} \qquad (4)$$

where N_A is Avogadro's Number and R is the Gas Constant. Since the ambient variables P and T always appear as a ratio it is convenient to define :

$$q = \frac{P}{T} \qquad (5)$$

Combining equations (2) – (5) yields :

$$\frac{\alpha}{q} = \frac{N_A \sigma}{R}\exp - \left(\frac{W N_A \sigma}{R\frac{E}{q}}\right) \qquad (6)$$

in which we see that α/q is a simple function of E/q, including both the electric field and the ambient dependencies. *E/q* is known as the *reduced electric field*. Comparing equation (6) with equation (2) shows that the quantity $\lambda q = R/N_A\sigma$ and equation (6) can be written as:

$$\frac{\alpha}{q} = \frac{1}{\lambda q}\exp\left(\frac{-W}{E/q\,\lambda q}\right) \qquad (6a)$$

where the parameters *W* and λq represent invariant physical parameters of the gas filling.

In equation (6) the electric field is in general a function of position, i.e. E = E(r). Substituting the appropriate function of E(r) for any given geometry of gas detector and integrating equation (1) with the functional dependence of α given in equation (6)

gives the equation describing the gas gain as a function of V_{ac} (the anode-cathode potential difference) and the ambient variable q.

2.1 The Single Wire Proportional Counter

The single wire proportional counter is generally taken as the canonical gas avalanche detector and it is the subject of most modelling studies. It consists of a fine wire of radius r_a stretched down the axis of a cylindrical tube of radius r_c which is filled with the active gas. A potential difference V_{ac} is applied between the electrodes with the wire positive with respect to the cathode. The electric field is radially symmetric and is described by:

$$E(r) = \frac{V_{ac}}{\ln(r_c / r_a) r} \qquad (7)$$

where r is the radial distance from the counter axis. Substituting this expression for E and integrating equation (1) from the cathode (r_c) to the anode surface (r_a) gives the gain formula. The rapid dependence of α on E(r) and the steep decline of E with r makes the integral insensitive to the cathode limit which is set to infinity in order to simplify the final expression:

$$\ln(M) = \frac{V_{ac}}{A} \exp\left(-\frac{AB}{V_{ac}} \right) \qquad (8)$$

where

and

$$A = W \ln(r_c / r_a) \ \text{(V)} \qquad (9)$$

$$B = \frac{r_a}{\lambda} = \frac{r_a N_A \sigma q}{R} \qquad (10)$$

In this (the simplest) version of the model the gain is entirely determined by the two parameters A and B with the gas thermodymamic dependence contained in B. Values of A and B obtained by fitting an experimental gain curve give directly the basic physical parameters W and λ by inversion of equations (9) and (10).

The gain of a single wire proportional counter consisting of a 20μm diameter gold-plated tungsten wire mounted axially in a brass tube of 20mm inner diameter and filled with a flowing argon + 7.5% methane gas mixture was studied. Figure 1 shows the measured data for the gain (plotted as lnM) as a function of the anode-cathode bias potential (V_{ac}) at constant q. Here it can be seen that equation (8) provides an excellent fit over a wide range of gain (70<M<17000) with fitted values: A = 75.367V and B = 13.788. Using the counter geometry and equations (9) and (10) we find W = 10.9eV and λ = 0.725μm. These are plausible values for an argon-based gas mixture at ambient conditions.

Equation (10) predicts that B should be a linear function of q. Figure 2 shows a plot of lnM as a function of q at V_{ac} = 1320V, taken over the range of q values accessible

in a flow counter due to changes in the ambient pressure and temperature (940mb<P<1030mb, 18C<T<24^{o}C). The data fits satisfactorily to a straight line function for the parameter AB/V_{ac}. However, the presence of a significant offset in the fitting function shows that the relationship predicted by equation (10) is not fulfilled exactly, and the fit is simply the local tangent to a curve which is gently concave down. This is an indication of the limitations of the model which will be discussed in detail below.

2.2 The GMSD

The GMSD consists of a pattern of interleaved, parallel metallic strips laid down on a semi-conducting glass surface [5]. A fine anode strip (typically 10μm wide(A_s)) is flanked by cathode strips which are typically ≈100μm wide (C_s), in a pattern which repeats every few hundred μm (i.e. pitch = P_s). In spite of the planar structure, the basic geometry of the avalanche region is similar to that of the single wire counter so it is not surprising that the gain of the GMSD fits well to equation (8). Figure 1 shows such a fit to experimental data from a GMSD.

Experiment shows that the electric field in the region in which the avalanche occurs near the GMSD anode strip is close to that of a cylindrical counter with $r_a = A_s/2$ and $r_c = (P_s-C_s)/2$. Thus equations (9) and (10) can be used for A and B. If this is done with the fit in figure 1, *W* is found to be 12.2eV and λ, 0.657μm, plausible values for operation at ambient conditions and close to that found above for the single wire counter.

The GMSD is usually operated as a three terminal device with a drift electrode placed parallel to the glass plate at a suitable (≈10mm) distance to define the active detector volume. As described in detail elsewhere [18], the drift electrode potential (V_d) contributes to the field in the avalanche region above the anode strip so that the correct bias for equation (8) is $V' = V_{ac} + \beta V_d$, where $\beta \approx 0.01$. Equation (8) generally achieves an excellent fit to the experimentally measured gain whether V_{ac} or V' is used (though, of course the fitted values of W and λ differ slightly).

It is noted in figure 1 that the bias potential required for GMSD operation is approximately one half that required for the single wire counter. This is, of course, simply a reflection of the difference of a factor of ≈50 in the anode-cathode gap of the two devices.

2.3 The Point Anode Detector

The point anode detector takes many detailed forms [3]; however, the basic element is a quasi-spherical anode structure near which the avalanches occur. For the purposes of modelling, the electric field near the anode is assumed to be that between two concentric spheres: the anode surface of radius r_a and the cathode surface of radius r_c. Thus:

$$E(r) = \frac{V_{ac}}{\left(\frac{1}{r_a} - \frac{1}{r_c}\right) r^2} \qquad (11)$$

The rapid dependence of E on r and the similarly rapid dependence of α on E (equation (2)) mean that the positioning and shape of the cathode generally have a weak effect on the gas gain and that the assumption of a spherically symmetric field near the anode is valid.

The gas gain is evaluated by substituting equations (11) and (2) in equation (1) and integrating. As in the wire counter case (and by the same justification), the integral is simplified by setting r_c to infinity. The result is :

$$\ln M = \frac{\sqrt{\pi}}{2} \sqrt{\frac{V_{ac}}{A}} erfc \sqrt{\frac{B}{V_{ac}}} \qquad (12)$$

where
$$A = \lambda W \left(\frac{1}{r_a} - \frac{1}{r_c}\right) \text{ (V)} \qquad (13)$$

and
$$B = \frac{W r_a^{\,2}}{\lambda} \left(\frac{1}{r_a} - \frac{1}{r_c}\right) \text{ (V)} \qquad (14)$$

Rearranging equations (13) and (14) gives :

$$W = \frac{\sqrt{AB}}{r_a \left(\frac{1}{r_a} - \frac{1}{r_c}\right)} \text{ (eV)} \qquad (15)$$

$$\frac{r_a}{\lambda} = \sqrt{\frac{B}{A}} \qquad (16)$$

erfc(x) is the complementary error function which requires a numerical integration for each evaluation. In order to simplify the fitting process using equation (12), *erfc(x)* is approximated by the expression:

$$erfc(x) \approx exp(-0.9062\, x^2 - 0.8751\, x) \qquad (17)$$

which gives a precision of a few % throughout the range $0 < x < 4$, in which the value of *erfc(x)* is significant.

Pin detectors use electronic connector pins to provide the quasi-spherical anodes of the counters. Figure 3 shows the fits of equation (12) to two pin detector designs. The right hand data set (squares) shows the gain curve of the imaging pin detector [19] which consists of a 2mm diameter ball connector mounted in a gas enclosure with the cathode readout structures at a distance of ≈30mm from the anode. It is operated in a

gas mixture of argon + 20% methane. A potential of $+V_{ac}$ is applied to the pin anode with the readout cathodes at earth potential.

Applying equations (15) and (16) to the fit parameters of the imaging pin detector data in figure 3 yields W = 28.8eV and $\lambda = 3.07\mu m$.

The array pin detector [20] is fabricated from an electronic connector array of 100 pins with hemispherical ends which are spaced at 2.54mm intervals on a grid. The pin tips are brought up close to a cathode plane with holes (aligned on the pins) through which the ionisation released in an active gas space are drawn into the avalanche region above each pin tip. The pins are held at earth potential and $-V_{ac}$ is applied to the cathode plane. The pin diameter is 0.48mm and the average distance to the cathode plane is ≈0.7mm (r_c = 1.02mm). The gain curve for a pin in this detector is shown as the open circles in figure 3 along with the fit to equation (12).

Applying equations (15) and (16) to the fit parameters of the array pin detector data in figure 3 yields W = 19.33eV and $\lambda = 1.83\mu m$.

The explicit dependence of the gain on the ambient variable q can be obtained by using equations (3) and (4) to substitute λ in equation (12).

2.4 The Parallel Gap Detector

In the parallel gap detector the avalanche takes place in the high electric field between two accurately parallel planar electrodes, the first of which is a form of mesh through which the x-ray generated ionisation may pass from the active volume of the detector into the high field region. In this case the electric field is uniform and given by:

$$E = \frac{V_{ac}}{d} \qquad (18)$$

where d is the separation between the anode and cathode planes. Substitution of this in equations (2) and (1) followed by integration leads to the relation:

$$\ln M = A \exp\left(\frac{-AB}{V_{ac}}\right) \qquad (19)$$

where

$$A = \frac{d}{\lambda} \qquad (20)$$

$$B = W \qquad (21)$$

The parallel gap detector used to produce the gain curve in figure 3 (filled circles) consisted of a 10mm deep conversion gap separated from a 1mm deep avalanche gap by a stainless steel mesh plane. The mesh was used as the readout electrode (at earth potential) and $+V_{ac}$ was applied to the rear foil electrode.

Applying equations (20) and (21) to the fit parameters of the parallel gap detector data in figure 3 yields W = 23.96eV and λ = 4.28μm.

3. Discussion of the Model

While the model clearly is capable of accurately fitting the gain curves of all the gas counters studied, its limitations are clearly seen in the systematic variation seen in the values of the two parameters *W* and *λ*, which should be invariant for a given gas. (Admittedly a variety of argon-based mixtures are used above, but the systematic variation clearly bears little relation to the changes in the gas mixture.) What is dramatically different in the various detectors is the value of the electric field near the anode (where the avalanche occurs). Table 1 shows λ and W tabulated against the anode field for all the devices tested. A clear picture emerges with λ smoothly increasing from 0.657μm (GMSD) to 4.28μm (parallel gap) as the reduced anode electric field decreases from 140 VK/(cm-mb) to 4.52 VK/(cm-mb). W shows a more erratic tendency to increase from ≈11eV to ≈25eV over the same range. This behaviour is clarified by comparison of the functional dependence for α given by equation (6a) with the experimental data for α available for argon [21].

Figure 4 shows that in the range of reduced field typical of wire and GMSD detectors ($>5x10^4$VK/(cm-mb)) α/q is well approximated by equation (6a) with W = 15.26eV and $\lambda q = 3.094x10^{-4}$, i.e. λ = 3.094/3.41 = 0.91μm, values similar to those observed with these detectors. In the region of reduced field typical of the pin and the parallel gap detectors ($10^3 – 10^4$ VK/(cm-mb)) the fit to the experimental data for α/q gives W = 27.83eV and λ = 0.001599/3.41 = 4.69μm. (Note: q = 3.41mb/K at 20^{o}C and 1000mb). Again these values tend to match to those obtained with the pin and parallel gap detectors (table 1).

These results inspire the search for a suitable functional form for W and λq as a function of the reduced field (X = E/q) so that the changes in the avalanche mechanisms with X can be satisfactorily captured by the simple model for α. Figure 5 shows the argon data modelled with the parameterisations:

$$W = a + b/X \qquad (22)$$

$$\lambda q = c + d/X. \qquad (23)$$

The resulting fit is excellent and the resulting functions W(X) and λq(X) are shown in figure 6. Figure 7 shows the same data plotted as W(X) and λ(X) (at ambient conditions: q = 3.41mb/K).

Bearing in mind that practical detectors always operate with variable fractions of various quenchers in the argon (which modify the situation a little), the message of figure 7 is that for most types of gas detectors which avalanche in reduced field values $>10^4$ VK/(cm-mb), the variation in W and λ is quite restricted. Given that the total avalanche process in a wire counter (for instance) occurs over at most a factor of three in X, the assumption of constant W and λ is not unreasonable and the success of the model is understandable.

In certain detectors it is possible to force the field configuration beyond that describable by the simple model. Figure 8 shows the gain curve of a GMSD design capable of giving a very wide range of gain (A_s = 5μm, C_s = 250μm, P_s = 500μm) [22] with the simple model not succeeding in fitting the data over the whole range. The parameterisation of W and λ derived above indicates an obvious generalisation of the basic gain formulae in equations (8)-(10). We now permit the gain constants A and B to be functions of V_{ac} of the form: $A = a + b/V_{ac}$ and $B = 1/(c + d/V_{ac})$. As figure 8 shows, this simple generalisation produces an excellent fit over the whole operating range of the detector.

4. The Extended Model

The success of the parameterisations for W and λq (specified in equations (22) and (23)) in representing the argon experimental data for α/q as a function of X (figure 5) points the way to an extended model for the avalanche gain process. The exact solution would involve substituting the relations (22) and (23) in equation (6a) which would be integrated according to equation (1). Such an integration could only be performed numerically and thus is of little use as a general tool. A simpler approximation to this process is indicated by the success of the fit to the GMSD gain data in figure 8 of the parameterisation of W and λq in terms of V_{ac}.

Noting that the avalanche takes place close to the anode and that the range of reduced field (X) in the avalanche region is not too great, we accept the gain equation calculated on the basis of constant W and λq and parameterise them in the gain formula with the functions defined in equations (22) and (23) with the X value set to that at the anode of the detector (X_a). Thus for the single wire proportional counter we can write:

$$X_a = \frac{V_{ac}}{r_a \ln(r_c / r_a) q} \qquad (24)$$

From equations (8) to (10) we can write:

$$\ln(M) = \frac{V_{ac}}{W \ln(r_c / r_a)} \exp\left(- \frac{W \ln(r_c / r_a) r_a q}{\lambda q V_{ac}} \right) \qquad (25)$$

Substituting relations (22) and (23) with $X = X_a$ we get:

$$\ln(M) = \frac{V_{ac}}{\{a + (bqr_a \ln(r_c / r_a)/V_{ac}\} \ln(r_c / r_a)} \exp\left(- \frac{\{a + (bqr_a \ln(r_c / r_a)/V_{ac}\} \ln(r_c / r_a) r_a q}{\{c + (dqr_a \ln(r_c / r_a)/V_{ac}\} V_{ac}} \right) \qquad (26)$$

This equation gives the explicit dependence of the gas gain on all the relevant variables in terms of four parameters: a,b,c,d which (in turn) define the behaviour of W and λq over a wide range of reduced field. While this formulation is still an approximation, it is reasonable to expect that it will be useful over a wider range of

operation than the simple model. The parameters a,b,c,d can be obtained by fitting them to a plot of lnM versus q using equation (26). Using the data of figure 2 for this purpose yields: $W = 9.99 + 1.927x10^4/X$ (eV) and $\lambda q = 1.32x10^{-4} + 4.985/X$ (mbcm/K).

Figure 9 compares the predictions of the extended model (equation (26)) and the simple model (equations (8) to (10) with constant W =10.33eV and $\lambda q = 2.21x10^{-4}$mbcm/K) for the gas gain of a single wire counter as a function of the wire radius (V_{ac} = 1320V). Both models produce a similar curve with good agreement in the region of high X (small anode radii) in which the calibration was made. However, for larger anode radii the two predictions diverge quite rapidly. This result simply confirms the expectation that the fixed W and λq of the simple model can only give accurate results when the range of X is restricted to the calibration region, though it gives the general behaviour over a wider range.

The parameterisations of W and λq in terms of the reduced anode field can be generated for the point anode and parallel gap counters in the same way as done above for the single wire cylindrical counter. Substitution in the gain formulae of the simple model then leads to the equivalent formulae to equation (26) for these cases.

5. The Ballistic Fraction

Gas avalanche counters (virtually without exception) are operated in pulse mode. In order to achieve this, some form of pulse shaping is applied to the charge waveform delivered by the detector; typically resistor-capacitor differentiation/integration (CR-RC). In this case the counter waveform is effectively sampled at a time τ (=RC) after the avalanche generated by the incident particle (e.g. x-ray). The formation of the charge waveform is governed by the movement (in the electric field of the detector) of the electrons and ions released in the avalanche. In devices which may be viewed as simple two-terminal capacitors, the charge induced on the electrodes may be deduced simply by considering the energy withdrawn by the drifting charges from the external power supply. The situation can be further simplified by the fact that the avalanche usually occurs very close to the anode so that the electrons have a very short distance to travel and they also have velocities which are (on average) hundreds of times greater than those of the ions. The problem thus reduces to consideration of the movement of the avalanche ion cloud from the anode to the cathode. This analysis is given in detail in reference [23].

The whole of the charge signal liberated in the avalanche is not available to the detecting circuits until the ions reach the cathode. This period is called the *positive ion transit time* (τ_I) and can range in value from μs to ms depending on the counter geometry. For practical purposes the amplifier shaping time τ is kept to ≈1μs or less and this generally means that only a fraction of the true avalanche gain is recorded. This is known as the *ballistic fraction*. For the simpler counter geometries the energy analysis permits the evaluation of the charge waveform from a fast event (such as an x-ray) Q(t) to be calculated. (The waveform generated by a charged particle (which can leave an extended trail of ionisation in the detector) is spread out by the drift of the primary electrons to the avalanche zone and is slower and more complex.) The results for three simplest cases are as follows:

Parallel Gap: $$\frac{Q(t)}{Q} = \frac{t}{\tau_I} \qquad (27)$$

Where: $$\tau_I = \frac{d^2}{\mu V_{ac}} \qquad (28)$$

Where Q is the total charge in the avalanche event, *d* is the width of the avalanche gap, μ the positive ion mobility and V_{ac} the potential difference across the gap.

Cylindrical Wire: $$\frac{Q(t)}{Q} = \frac{1}{2\ln(r_c / r_a)} \ln\left(1 + \frac{t}{\tau_R}\right) \qquad (29)$$

where

$$\tau_R = \frac{r_a{}^2 \ln(r_c / r_a)}{2\mu V_{ac}} \qquad (30)$$

and τ_R is the parameter which determines the fast part of the waveform. The expression (29) attains unity at the ion collection time:

$$\tau_I = \frac{r_a{}^2 \ln(r_c / r_a)\left\{r_c{}^2 - r_a{}^2\right\}}{2\mu V_{ac}} \qquad (31)$$

In general $r_c >> r_a$, it follows that:

$$\tau_R \cong \frac{r_a{}^2 \tau_I}{r_c{}^2} \qquad (32)$$

Spherical Electrodes:

$$\frac{Q(t)}{Q} = \frac{1}{(1 - r_a / r_c)}\left(1 - \frac{1}{(1 + t/\tau_R)^{1/3}}\right) \qquad (33)$$

Where: $$\tau_R = \frac{r_a{}^3 (1/r_a - 1/r_c)}{3\mu V_{ac}} \qquad (34)$$

And: $$\tau_I = \frac{(r_c{}^3 - r_a{}^3)(1/r_a - 1/r_c)}{3\mu V_{ac}} \qquad (35)$$

If $r_c >> r_a$, then $$\tau_R \cong \frac{r_a{}^3 \tau_I}{r_c{}^3} \qquad (36)$$

These formulae can be used to estimate the charge waveforms of x-ray pulses in the different detectors (of which the gain curves are presented in figures 1 and 3) with varying degrees of precision as figure 10 shows. Within the limitation of the assumption of the ion mobility of argon ions for all the different ions present ($\approx 1.7 cm^2/(Vsec)$), the representation of the cylindrical wire counter, the parallel gap counter and the imaging pin counter are essentially accurate on the time scale presented in figure 10. (V_{ac} is chosen at a typical operating point of each detector.) In the pin array detector the ions are collected by both the cathode and the drift electrode. However, since a low drift field is generally used, most go to the cathode and the curve in figure 10 will be reliable in the first microsecond or so which concerns us.

In the GMSD, drift fields are generally high with a large proportion (>50%) of the ions travelling to the drift electrode. The structure of the field pattern near the anodes approximates to that of a cylindrical detector of cathode radius $(P_s-C_s)/2$ (see section 2.2 above) with a typical τ_I of a few hundred ns, and that in the drift section to a parallel gap with a typical τ_I of a few hundred μs. Fortunately the electrode pattern on the GMSD plate (with much more cathode area than anode area) functions as a Frisch grid and ensures that the very slow component of Q(t) is very small indeed (a few percent). The complex field structure of the GMSD means that a full numerical solution (using Greens theorem) is required to calculate Q(t) and no simple formulae are possible. The numerical solution of Bellazzini and Spezziga [24] for a typical GMSD structure is shown in figure 10. It shows that there is a sharp rise to about 95% in about 200ns followed by a very slowly rising plateau which is estimated to terminate at 100μs. In fact the front edge can be fitted quite accurately with the form of equation (29), but only up to t≈200ns.

Table 2 summarises the numerical values of τ_R and τ_I for all the detectors. Here we see an important characteristic of gas avalanche counters, namely the very large ratio which generally exists between the fast part of the pulse and the final ion collection time. The build up of positive ion space charge in the long drift is one of the limiting rate factors on the counter as it eventually distorts the counter electric field and depresses the gain.

With amplifier shaping time constants (τ) of 1μs, the ballistic fraction (F_B) for each counter can be read off each plot as the value of Q(t)/Q at t = 1μs. In figure 10 F_B varies from 25% for the parallel gap counter to 96% for the GMSD, showing what a significant effect that it has on the gain calibration. Further, τ_R is a linear function of V_{ac} so that F_B can change significantly over the operational bias range. In order to produce corrected gain curves, the data of figures 1 and 3 were divided by the function Q(1)/Q as a function of V_{ac} (of the corresponding counter) and the new gain curves fitted as described in section 2 above to generate new values of W and λ. Table 3 shows the resulting values which demonstrate a systematic increase in both parameters for all detectors, the smaller F_B, the larger the change. Only the GMSD which has F_B close to unity shows negligible change. (Because no formulae is available for Q(t)/Q in this case and the correction is very small, a constant value of F_B was used throughout the range of V_{ac}.)

Figure 11 shows these corrected values of W and λ plotted against the anode reduced field for all the detectors. The λ values fit reasonably well to the expected function

(equation (23), but the W values fall into two groups depending on the quencher concentration. Thus the two points taken with 7.5% methane can be seen to be consistent with a different curve (equation (22)) to that for the curves with 20-25% of quencher. The increase of W with the quencher concentration is a reflection of the large inelastic scattering cross-section of the quencher compared with argon.

The dependence of τ_R on the ion mobility (μ) makes F_B sensitive to changes in the pressure (P) and (absolute) temperature (T) of the gas. Elementary kinetic theory shows that this dependence is:

$$\mu \propto \frac{T^{1/2}}{P} \qquad (37).$$

If the amplifier time constant τ is below the knees of the Q(t) curves (figure 10) (or τ_I in the case of the parallel gap) then the apparent gain of a gas counter will decrease with increasing gas pressure rather faster than indicated by the basic gain model.

Figure 10 also shows the flexibility of point and line anode designs, in that there is always a relatively fast (sub μs) rise to the charge pulse over a wide range of anode dimensions so that a reasonable fraction of the charge signal is available (≈50%). With parallel gap counters the gap dimension is critical and must be sub-millimetre if microsecond pulses are to be used.

6. Applications of the Model

It is clear from the above discussion that the pulse gain available from any gas avalanche detector is accurately described by the simple models developed in section 2 only if the ballistic fraction F_B remains roughly constant and the reduced anode electric field X_a does not vary by a large factor over the range of study. The first condition can be met by ensuring that the amplifier shaping time constant τ is long enough that the peak sampling time is above the knee of the $Q(t)/Q_0$ curve throughout the study range. If the range of X_a is large (decades) then the extended model must be used and the parameters a,b,c,d evaluated for accurate modelling. However, as figure 9 shows, the simple model is capable of representing the general behaviour of the gain over 3 decades of X_a with the main caveat being that it systematically underestimates it at the lowest reduced field values (largest radii in figure 9).

6.1 Gain as a Function of Anode Dimension

Accepting the limitations noted above, the simple model can be used to compare the gain of the three types of avalanche counters as a function of their anode dimension. Using the fit parameters W and λ derived from the experimental data of figures 1 and 3, the gain formulae (8), (12) and (19) are used to plot the gain of the wire counter, pin detector and parallel gap as a function of the wire radius, pin radius and gap width – figure 12. All the detectors display the same characteristic behaviour with the gain peaking at a wire radius of 0.9μm, a pin radius of 36μm and a gap width of 111μm. The bias potential has been chosen so as to give a gain of ≈10000 in each case.

The plots of figure 12 imply that there is an optimal design for each type of detector, if for no other reason than the fact that at the peak of the gain curve each detector is maximally insensitive to dimensional irregularities in the gain-determining structure. Since it is easy to generate GMSD anodes of various widths using the lithographic process, the gain of GMSD anodes of width 2,3,4,5 and 10μm was measured. Figure 13 shows the result with the gain peaking at an anode width of 3μm (radius = 1.5μm) and the gain curve fitting reasonably well to the approximate wire formula given in section 2.2. The optimal radius from the GMSD data (1.5μm) is larger than the prediction of figure 12 (0.9μm); however, as noted above, precise agreement is not to be expected and the order of magnitude is satisfactory.

6.2 Counter Spark Stability

The high gain of gas counters means that sparking is inevitable if any positive feedback processes arise. Typically these are electron photo-emission, field emission and electron emission from neutralising ions at the cathode. These processes are sensitive to the electric field strength (E_c) at the cathode and it is generally found that this parameter is a good diagnostic of the maximum gain from a detector (when other things such as the gas mixture are equal). In figure 14 the simple model for the wire counter is used to calculate V_{ac} and thence E_c using the relation:

$$E_c = \frac{V_{ac}}{r_c \ln(r_c / r_a)} \qquad (38)$$

in the case that a constant gain of M=5000 is demanded. (Since formula (8) cannot be inverted simply, this is done numerically.) Figure 14 shows that the cathode field decreases monotonically with the anode radius and, at the maximum of the gain curve in figure 12, E_c is below 100V/cm. This behaviour illustrates the well-known design criterion that high gain wire counters should have very small anode wire diameters.

In the GMSD the effective r_c decreases to fractions of a millimetre and the stability correspondingly decreases. The different geometry means that E_c is determined as much by the width of the cathode strip as the anode-cathode gap. This behaviour is demonstrated in the results presented in reference [22]. However, as the data in figure 13 shows, the maximum gain rises steadily as the anode width decreases.

As an aside we note that the parameters determining the ballistic fraction τ_R and τ_I (equations (30) and (31)) both vary as $r_a^2 \ln(r_c/r_a)$ and so F_B also increases as the anode radius decreases.

The same argument holds *a fortiori* for the pin detector since the electric field in the anode-cathode space falls off as $1/r^2$, making E_c very low. The pin array reduces this stability somewhat by bringing the intermediate cathode to within ≈1mm of the pin tips.

The situation is very different in the parallel gap detector in which the full anode field strength required for the avalanche is present at the cathode electrode. Equation (19) may be simply inverted to get V_{ac} as a function of M and hence the gap field E_g ($=V_{ac}/d$). Explicitly this is:

$$E_g = \frac{Wq}{\lambda q}\frac{1}{\{\ln(qd/\lambda q) - \ln(\ln M)\}} \qquad (39).$$

Figure 15 shows a plot of E_g as a function of the gap width d at a constant gain of M=5000. In this case the gap field **increases** monotonically as the gap width decreases and at the maximum of the gain curve in figure 12, has a value of 6 x10^4 V/cm. This graph shows why it is, in general, difficult to get stable, high gains from parallel gap detectors. The high cathode field strengths impose very limiting conditions on the quality of the electrodes and the quenching capacity of the gas.

6.3 Design Criteria for Micromegas.

Micromegas is a parallel gap detector with an avalanche gap of dimensions less than 1mm [25]. The simple model is useful for evaluating some of the important operating parameters of the device. Figure 12 shows that using the parameters derived from the detector with a gap of 1mm, there is a maximum in the gain versus gap curve at d=111μm (for a gain of 9000) and it is interesting to look at the properties of the device around the gain maximum. From equation (19) we can write explicitly:

$$\ln M = \frac{qd}{\lambda q}\exp\left(-\frac{Wqd}{\lambda qV}\right) \qquad (40)$$

where the explicit product λq is retained as an approximate invariant, and V is the potential difference across the avalanche gap. Differentiating with respect to d we get:

$$\frac{1}{M}\frac{\partial M}{\partial d} = \ln M\left(\frac{1}{d} - \frac{Wq}{\lambda qV}\right) \qquad (41)$$

The gain maximum in figure 12 is now identified by setting $\frac{1}{M}\frac{\partial M}{\partial d} = 0$, giving the position of the maximum:

$$d_{\max} = \frac{\lambda qV}{Wq} \qquad (42)$$

i.e. the gap required for the gain maximum varies linearly with the operating potential. Thus in order to sit on the maximum, a unique potential and thus gain is determined. It also follows from equation (42) that the electric field in the gap is the same whenever a gap is operated on the peak: i.e. $E_g = Wq/\lambda q$. Using the experimental parameters from the 1mm gap this evaluates to $E_g = 5.33 \times 10^4$V/cm.

By eliminating V from equation (41) by substituting from equation (40) we can quantify the gain stability as a function of the gap width at a given operating gain:

$$\frac{1}{M}\frac{\partial M}{\partial d} = \frac{\ln M}{d}\left(1 + \ln(\ln M) - \ln\frac{qd}{\lambda q}\right) \qquad (43)$$

This function is plotted in figure 16 with M = 5000, q = 3.41mb/K and $\lambda q = 1.529\text{x}10^{-3}$cmmb/K. As expected, the differential is zero at the gain maximum. However, the very asymmetric behaviour either side of the peak means that if a variable gain is desired from the detector it is clearly preferable to choose the gap so that the operating region lies (effectively) on the upper side of the gain maximum on this plot. In the gap range 100μm to 1mm the relative differential is moderately uniform with a maximum of 300cm^{-1}. This translates into a gain variation of 3% per μm of change in d. Since x-ray pulse height spectra in gas counters generally have a spread of ≈10% FWHM or greater, this means that fluctuations of a few μm are tolerable in the gap so operation exactly on the gain maximum is not necessary if this tolerance can be achieved.

It is often desirable to operate gas counters with flowing gas. In this case the gain becomes sensitive to the ambient variable q. In order to quantify this we differentiate Equation (40) with respect to q:

$$\frac{1}{M}\frac{\partial M}{\partial q} = \frac{\ln M}{q}\left(1 - \frac{Wqd}{\lambda q V}\right) \qquad (44)$$

It is immediately obvious that substituting d_{max} from equation (42) into equation (44) makes the differential zero, so that by operating at the gain maximum, one can obtain complete immunity from q shifts. Eliminating V from equation (44) in favour of lnM gives the behaviour of this differential as a function of the gap width:

$$\frac{1}{M}\frac{\partial M}{\partial q} = \frac{\ln M}{q}\left(1 + \ln(\ln M) - \ln\frac{qd}{\lambda q}\right) \qquad (45)$$

Figure 17 shows the plot of this function with the gain fixed at M = 5000 and the same experimental parameters as before. In this case the obvious operating point is as close to the gain maximum as possible. Allowing for a reasonable operating range in gain and for the sensitivity of the gain maximum to q, it should be possible to keep the relative differential to the order of 1K/mb which is the level of stability achieved by a wire counter. This gives a gain shift of ≈0.3% per K and 0.1% per mb.

The maximum of the gain curve in figure (12) represents a triple point characterised by the variable values (V_{max}, d_{max}, M_{max}) which are all uniquely determined by the gas and ambient variables (W,λq,q). Combining equations (40) and (42) gives the complete specification:

$$V_{max} = \exp(1) W \ln(M_{max}) \qquad (46)$$

and,

$$d_{max} = \exp(1)\frac{\lambda q \ln(M_{max})}{q} \qquad (47)$$

Since the practical design situation requires a specified gas gain, the gain is used as the independent parameter. If equation (47) is inverted, it is obvious that M_{max} is an exponential function of d_{max}. Thus reducing the gap width rapidly reduces the gain available at the desirable triple point operating conditions.

6.4 Gain Stabilisation of Flowing-gas Counters

In the case of the wire counter, writing out equation (8) explicitly we have:

$$\ln M = \frac{V_{ac}}{W \ln(r_c / r_a)} \exp\left\{ -\frac{\left(W \ln(r_c / r_a) r_a q\right)}{\lambda q V_{ac}} \right\} \qquad (48)$$

where λq is again retained as an approximate invariant.

Equation (48) shows that M is a function of V_{ac} and q so that an excursion in M is given by :

$$dM = \frac{\partial M}{\partial V_{ac}} dV_{ac} + \frac{\partial M}{\partial q} dq \qquad (49)$$

Since the term on the left of equation (48) is ln M, it is more appropriate to write (49) as:

$$\frac{dM}{M} = \frac{1}{M}\frac{\partial M}{\partial V_{ac}} dV_{ac} + \frac{1}{M}\frac{\partial M}{\partial q} dq \qquad (50)$$

The servo condition for using V_{ac} to stabilise the changes in q is:

$$\frac{dM}{M} = 0 \qquad (51)$$

Or :

$$\frac{1}{M}\frac{\partial M}{\partial V_{ac}} dV_{ac} = -\frac{1}{M}\frac{\partial M}{\partial q} dq \qquad (52)$$

giving us the differential equation :

$$\frac{dV_{ac}}{dq} = -\frac{\frac{1}{M}\frac{\partial M}{\partial q}}{\frac{1}{M}\frac{\partial M}{\partial V_{ac}}} \qquad (53)$$

For convenience we write :

$$S = -\frac{\frac{1}{M}\frac{\partial M}{\partial q}}{\frac{1}{M}\frac{\partial M}{\partial V_{ac}}} \qquad (54)$$

And so integrating equation (53) we get the servo relation :

$$V_{ac} = V_0 + S(q - q_0) \qquad (55)$$

Where V_0 and q_0 are operating bias and ambient conditions to which we wish to servo the gain. This is a particularly simple (linear) correction function provided the function S is effectively constant over the range of V_{ac} and q met with in practice. The following analysis shows that this is in fact the case and experiment confirms it also.

Differentiating equation (48) with respect to q gives :

$$\frac{1}{M}\frac{\partial M}{\partial q} = -\frac{W \ln(r_c / r_a) r_a}{\lambda q V_{ac}} \ln M \qquad (56)$$

and with respect to V_{ac} gives :

$$\frac{1}{M}\frac{\partial M}{\partial V_{ac}} = \ln M \left(\frac{1}{V_{ac}} + \frac{W \ln(r_c / r_a) r_a q}{\lambda q V_{ac}^{\ 2}} \right) \qquad (57)$$

Substituting relations (56) and (57) into (54) yields :

$$S = \frac{W \ln(r_c / r_a) r_a}{\lambda q \left(1 + \frac{W \ln(r_c / r_a) r_a q}{\lambda q V_{ac}} \right)} \qquad (58)$$

In order to evaluate S an actual case must be considered. In the Wide Angle X-ray Scattering (WAXS) detector [26] operating with 17% dimethylether (DME) in argon at a gain of M = 1080, V_{ac} = 500V and fitting to equation (48) gives $\frac{W \ln(r_c / r_a) r_a q}{\lambda q} =$ 174V. Since the second term in the denominator of equation (58) is < 1 (0.348), the effect of the small changes in q and V_{ac} involved in the process are attenuated and, further, the sense of change of V_{ac} in the servo process follows that of q so minimising any change in S throughout the parameter range required by the servo process.

Thus, the simple linear relation of equation (55) can be used to perform the stabilisation of the gain against the effect of changes in ambient conditions, using only a single constant S, which can be evaluated by the following simple calibration.

In order to evaluate the key servo parameter S it is necessary to evaluate the two parameters $\frac{1}{M}\frac{\partial M}{\partial q}$ and $\frac{1}{M}\frac{\partial M}{\partial V_{ac}}$ near the desired operating point q_0. The simplest way to do this is to note that if a fit of the form $M = a\ exp(bx)$ is made to any gain function M(x) then $\frac{1}{M}\frac{\partial M}{\partial x}$ is simply the parameter *b* in the exponential fit. In view of the approximate constancy of S, it is not necessary to be excessively precise about the reference values of the second variable in each data set. It is also clear that in measuring *b*, the units of the ordinate are immaterial and there is no need to calibrate the gain. However, when working directly in PHA channels it is important to ensure that any digital offset has been measured and removed from the peak channel data.

The b parameters of the fits obtained from the WAXS detector data [27] allow us to evaluate S = 0.767/0.0189 = 40.58VK/mB and a servo function of:

$$V_c = 490 + 40.58(q - 3.411)V \qquad (59)$$

Where q_0 is set arbitrarily to P = 1000mb and $T = 20^oC$.

Figure 18 shows how the counter gain (circles) is controlled against changes in the ambient variable (q) when this condition is applied. The RMS error on the controlled mean gas gain of 754.56 is 4.64 giving a fractional error of 0.62%. This is achieved over a range of q corresponding to 986<P<1017mbar and 16.4<T<26.4^{o}C. The unstabilised gain (squares) at V_c=490V is also shown for comparison.

6.5 Operating Gas Counters away from Ambient Conditions.

One of the outstanding advantages of gas counters is their ability to function with a wide range of gas fillings at ambient, hyperbaric (above ambient) or hypobaric (below ambient) pressures. Hyperbaric operation is often used to enhance the detection efficiency for high energy x-rays and neutrons, while hypobaric operation is often used for the detection of ultra-violet light. Potential uses of the gain model are the analysis of gain data over a wide range of q and prediction of the gain outside the calibration range when required. Suitable data is available for analysis from the work of Shekhtman and his collaborators [28] who tested a GMSD with a hyperbaric xenon filling.

Figure 19 shows the avalanche gain curves presented in reference [28] for a GMSD with a pattern pitch (P_s) of 200μm, an anode width (A_s) of (3μm) and a cathode width of 60μm, operated with a filling of xenon + 20%CO_2 at pressures of 1.2, 2, 3, 4, 5, 6 bars. The analysis uses the simple version of the model to provide smooth fits to the sparse data (figure (19)) so that interpolated gain values can be obtained at a fixed V_{ac} (630.5V) to provide a plot of lnM versus q over the operating range. This plot is shown in figure 20. This data can now be used to fit lnM to q using equation (26) (the extended model) and so obtain the constants a,b,c,d. (The GMSD approximations for r_a and r_c of section 2.2 are used.) Before attempting the fit, equation (26) is simplified as follows:

$$\ln M = \frac{V_{ac}}{(\alpha + \beta q / V_{ac})} \exp\left\{ - \frac{(\alpha + \beta q / V_{ac}) q}{V_{ac} (\gamma + \delta q / V_{ac})} \right\} \qquad (60)$$

where:

$\alpha = a\ ln(r_c/r_a)$, $\beta = b r_a\ (ln(r_c/r_a))^2$, $\gamma = c / r_a$, $\delta = d\ ln(r_c/r_a)$.

For practical purposes, there is no need to unscramble the variables, *a,b,c,d* unless explicit representations are required for W and λq. The fit of equation (60) is shown in figure 20. The fitted values of α,β,γ,δ can now be used to predict the gain curves as a function of V_{ac} for the different pressures. Figure 21 shows the predictions superimposed on the experimental data.

As figure 21 indicates, the agreement of the model with the data is good up to a pressure of 3bar, but consistently overestimates the gain at the higher pressures. One reason for this is the fact that the fitting process (lnM versus q) was only carried out at a single value of V_{ac} at the low end of the data set so there is every reason to expect the extrapolation to drift away at the other extreme of the set. Ideally the fit of lnM to q would be carried out by optimising over both V_{ac} and q simultaneously over the full range of both variables.

A further consideration is the effect of the gas pressure on the ion mobility and hence the charge pulse risetime τ_r (equation (30)). The risetime τ_r is proportional to P/V_{ac} and inspecting figure 21 we see that at the maximum gain used τ_r increases by a factor of just over three between P = 1.2bar and P = 6bar. The amplifier shaping time constant is not known, but as the GMSD is designed for fast counting, it may be assumed to be short and in this case could lead to a significant decrease in the ballistic fraction F_B at the higher gas pressures. This would reproduce the type of disagreement seen in figure 21 at the higher pressures.

The necessity of the extended model when covering a large range of q is seen if one considers the prediction of equation (57) for V_{ac} in the WAXS GMSD for operation at a pressure of 6bars (remember this relation is only calibrated for use close to ambient pressure). It predicts a rise of a factor of 2.4 in V_{ac}. As we see from figure 21, the increase in V_{ac} observed in the xenon GMSD is only a factor of 1.6. This difference is caused by the dependence of W and λq on the reduced anode electric field (equations (22) and (23)).

As seen in figure 12, all detector types have an optimum anode dimension at which the gain maximises at a fixed V_{ac}, and the various operating parameters tend to optimise. The simpler mathematics of the parallel gap case shows that this condition is in fact a triple point at which the three parameters V_{max}, d_{max} and M_{max} are locked together. Equation (47) shows that d_{max} is inversely proportional to q. Although similar simple explicit relations cannot be produced for the wire (GMSD) and spherical anode devices, their behaviour is inevitably parallel. Thus, in general we expect that the optimum anode structure will decrease in size as q increases. In figure 22 the parameter fits to equation (26) from the data of figure 2 are used to predict the behaviour of the gas gain of a wire counter with r_c = 1cm operated at V_{ac} = 1320V in argon + 7.5% methane at a range of gas pressures as the anode radius is varied.

Typically, the optimum anode radius decreases to sub-micron values as the pressure rises above ambient. Conversely, in hypobaric operation, the anode dimension should be increased.

The GMSD is a technology which can realise such narrow anode widths. However, as the gas pressure rises, the destructive potential of sparks increases and the low mass of metal in the track makes it extremely vulnerable to spark damage. Using the same modelling data as used in figure 14 to predict the cathode electric field we find that for a fixed gain, V_{ac} minimises at the gain maximum. The stored energy available to the spark is $\frac{1}{2}CV_{ac}^2$ where C is the total stray capacity of the anode structure. Thus, provided the value of C is kept to a minimum operation at the triple point is favourable. A further protective mechanism is available in the choice of the metal of the anode strip; a resistive metal such as chromium can be used to limit the spark currents.

The optimal operating conditions of a parallel gap counter under hyperbaric operation are predicted by the simple model in equations (46) and (47). The simple model predicts a linear decrease in d_{max} as the pressure (i.e. q) is increased. The effect of the increase in λq with q (as predicted by the extended model) can be seen to cancel out some of this decrease, so that the effect of pressure change is not as extreme as this. However, for typical avalanche gains ($M \approx 5000$) the parallel gap will decrease to much less than 100μm for significant over-pressures. As noted in section 6.3, the gap electric field $E_g = Wq/\lambda q$ and so increases approximately linearly with q (W and λq vary in the same sense with q – see figure 6). Thus values of $E_g > 10^5$ V/cm are easily exceeded and the stored energy per unit area of gap ($\frac{1}{2}\varepsilon_0 E_g^2 d_{max}$) rises proportionately. Thus, while the grids of the parallel gap structure may be more robust than the anode strips of the GMSD, the immunity to spark damage may not be any better and the stability of the counter against sparking is liable to be considerably poorer in hyperbaric operation.

6.6 Gain Variation with Gas Composition.

It was noted in section 3 that W and λq are pseudo-physical parameters, and that, in combination they represent the behaviour of the competing inelastic electron scattering processes in the gas. The presence of a quencher component in the counter gas is essential for stable avalanche operation at useful gas gains. However, the quencher, by its very nature, introduces a series of inelastic scattering processes, which result in the gain of the counter being sensitive to the fraction of quencher in the gas mixture. Figure 23 shows a series of gain curves obtained from a GMSD as the fraction of isobutane quencher in argon is increased from 5% to 100%. Using the simple model, gain fits to all the data sets are made and the values of W and λq extracted using the relations (8), (9), (10) with the GMSD approximations of section 2.2. Figure 24 plots the derived values of W and λ as a function of the quencher fraction.

In figure 24 we note that as the quencher fraction tends to zero W tends to ≈14ev which is close to the ionisation potential of argon. However, in pure isobutane, W = 24.5eV which is many times the ionisation potential of isobutane. This behaviour

reflects the large number of dissipative inelastic interactions possible in isobutane (e.g. vibrational and rotational modes).

The results shown in figures 23 and 24 have obvious practical implications for counter operation: The highest gain data point in each curve represents the highest stable gain obtainable with that gas mixture. Inspection shows that the maximum gain is available at an isobutane fraction of 75%. Since the UV absorption of the quencher is proportional to its density, it follows that for hyperbaric operation the fraction can be reduced in proportion to the pressure (i.e. the partial pressure of the quencher is kept constant). Thus if operation is required at 5bar, the fraction of isobutane need only be 5% instead of the usual 25%. As figure 23 shows, this adjusts W and λq in such a way as to achieve a gain of 1000 at a bias potential of 476V instead of 630V, reducing the stored energy by almost a factor of two. The reduction in the maximum gain available is usually not a problem as the neutrons or high energy x-rays being detected give large pulse heights.

7. Conclusions.

Mathematical models of the avalanche gain process have been developed for all the typical gas counter geometries. Based on the pseudo-physical parameters W (the notional ionisation threshold energy) and λq (proportional to the inelastic electron scattering cross-section) the simple models have been shown to work well for typical counter operation around ambient conditions when W and λq may be assumed to be constant. Comparison of the Townsend coefficient of argon with the form used in the model shows that W and λq can be represented as simple functions of the reduced electric field X, (equations (22),(23)). Since the avalanche takes place in the electric field close to the cathode the corrected values of W and λq can simply be represented in terms of the anode potential, V_{ac}, q and four new constants. Incorporating these formulations of W and λq into the simple models leads to the extended models, of which equation (26) is an example. The extended models can now be used to characterise the gain performance of the various counter types over the widest range of operating conditions, examples of which have been given.

Careful consideration has been given to the effect of the finite charge collection times (ballistic fraction) on the evaluated parameters (W and λq). For reliable use of the gain models it is necessary to ensure that the pulse amplifier shaping time is long enough to ensure that the sampling time is above the knee of the charge delivery time curve Q(t) throughout the operational range (figure (10)).

Application of the models to the design of gas counters shows that (for fixed gas conditions) all possess an optimal anode dimension (figure (12)). This is a triple point with the gain, operating potential and anode dimension locked together. In ambient conditions, the typical optimal anode dimensions are ≈1μm radius for a wire (microstrip) detector, ≈40μm radius for a point anode detector and ≈100μm for a parallel gap detector. The optimal dimension varies inversely with the gas pressure (i.e. q) (equation (47)). At the triple point the differential sensitivity to dimensional and ambient changes tend to be minimised, and, in the case of wire, strip and point detectors, the electric fields minimised.

Throughout the analysis the gas ambient variable q (=P/T) has been used. This ensures that the formulations may be applied equally to sealed counters (when the density, and hence λ are temperature invariant) and flow counters when the temperature must also be taken into account.

References

1. G. Charpak, W. Dominik, J.C. Santiard, F. Sauli and N. Solomey, Nucl. Instr. and Meth. A274 (1989) 275-290

2. S.C. Curran and J.D. Craggs, Counting Tubes, Butterworth, London, 1949

3. G. Comby et. al. CEN-Saclay report DphE/STIPE 79/01/02/36
G. Comby and P.Mangeot, IEEE Trans. Nucl. Sci. NS-27 (1980) 106

4. F. Bartol et al, J Phys III France 6 (1996) 337

5. A. Oed, Nucl. Instr. and Meth. A263 (1988) 351-359

6. S. F. Biagi and T. J. Jones, Nucl. Instr. and Meth. A361 (1995) 72-76

7. M. E. Rose and S. A. Korff, Phys. Rev. 59 (1941) 850

8. W. Diethorn, NYO-6628 (1956)

9. A .Williams and R .I. Sara, Int. J. Appl. Rad. Isotopes 13 (1962) 229

10. A. Zastawny, J. Sci. Instr. 43 (1966) 179

11. M. W. Charles, J. Phys. E 5 (1972) 95

12. W. Bambynek, Nucl. Instr. and Meth. 112 (1973) 103

13. R. S. Wolff, Nucl. Instr. and Meth. 115 (1974) 461

14. J. Planinic, Nucl. Instr. and Meth. 136 (1976) 165

15. H. Miyahara, M. Watanabe and T. Watanabe, Nucl. Instr. and Meth. A241 (1985) 186-190

16. Y. Uozumi, T. Sakae, M. Matoba, H. Ijiri,, N. Koori, Nucl. Instr. and Meth. A324 (1993) 558-564

17. J.A. Crowther, Ions, Electrons and Ionising Radiations, Edward Arnold, London 1959

18. J. E. Bateman, J. F. Connolly, G. E. Derbyshire, D. M. Duxbury, J. Lipp, J. A. Mir, R. Stephenson, J. E. Simmons and E. J. Spill, Studies of the gain properties of gas microstrip detectors relevant to their application as x-ray and electron detectors,

RAL-TR-1999-057 (http://www-dienst.rl.ac.uk/library/1999/tr/raltr-1999057.pdf), to be published in IEEE Trans. Nuc. Sci.

19. J. E. Bateman, The Imaging Pin Detector - a simple and effective new imaging device for soft X-rays and soft beta emissions, Nucl. Inst. and Meth. A240 (1985) 177-187

20. J.E.Bateman, J.F.Connolly, G.E.Derbyshire, D.M.Duxbury, A.S.Marsh, J.E.Simmons and R.Stephenson, The Pin Pixel Detector – X-ray imaging, Rutherford Appleton Laboratory Report, RAL-TR-2001-009, (http://www-dienst.rl.ac.uk/library/2000/tr/raltr-2001009.pdf), to be published in Nucl. Instr. and Meth.A

21. S.C. Brown, Basic Data of Plasma Physics, MIT Press, Cambridge Mass, 1959

22. J.E.Bateman, R.Barlow, G.E.Derbyshire, J.A.Mir and R.Stephenson, Optimising the design of gas microstrip detectors for soft x-ray detection, Rutherford Appleton Laboratory Report, RAL-TR-2001-008, (http://www-dienst.rl.ac.uk/library/2000/tr/raltr-2001008.pdf), to be published in IEEE Trans. Nuc. Sci.

23. F. Sauli, Principles of operation of multiwire proportional and drift chambers, CERN 77-09

24. R. Bellazzini and M.A. Spezziga, Revista del Nuovo Cimento 17 (1994) 1-91

25. Y. Giomataris, Ph. Rebourgeard, J.P. Robert and G. Charpak, Nucl. Instr. and Meth. A376 (1996) 29

26. J E Bateman, J F Connolly, G E Derbyshire, D M Duxbury, J Lipp, J A Mir, J E Simmons, E J Spill, R Stephenson, R C Farrow, W I Helsby, B R Dobson, R Mutikainen and I Suni, A gas microstrip wide angle x-ray detector for application in synchrotron radiation experiments, Nucl. Instr. and Meth. A477, (2002), 29-36

27. J.E. Bateman and D.M. Duxbury, Calibration of the servo equation for a gas microstrip detector, Rutherford Appleton Laboratory report RAL-TR-2001-038, (http://www-dienst.rl.ac.uk/library/2000/tr/raltr-2001038.pdf)

28. G.D. Minakov, Yu.N. Pestov, V.S. Prokopenko and L. I. Shekhtman, Nucl. Instr. and Meth. A326 (1993) 566-569

Figure Captions

1. The gas gain curves (lnM versus V_{ac}) for a single wire cylindrical proportional counter and a gas microstrip detector (GMSD) with the corresponding fits of the simple gain model.

2. A plot of the logarithm of the gas gain of the wire counter as a function of the gas ambient variable q (=P/T) over the range experienced by a flow counter due to ambient changes in P (pressure) and T (absolute temperature).

3. A plot of the gain curves (lnM versus V_{ac}) for a parallel gap counter, the 10x10 pin array [20] and the imaging pin detector [19] with the corresponding simple model fits.

4. A comparison of the reduced (first) Townsend coefficient of argon with the simple model with two sets of fixed values of W and λq corresponding to the typical reduced electric field X (=E/q) in the wire counter and the parallel gap counter.

5. A fit of the argon Townsend coefficient over the whole range of X with the parameterisations of W(X) and λq(X) used in the extended gain model (equations (22), (23).

6. A plot of the fits of W(X) and λq(X) to the argon data.

7. A plot of the fits of W(X) and λ(X) to the argon data in ambient conditions.

8. The gain versus bias (V_{ac}) data for a GMSD operating over a very wide gain range [22] with a simple model fit (dashed line) and a simple parameterisation of A and B in terms of V_{ac} suggested by the W(X), λ(X) functions.

9. A comparison of the gain versus anode radius plots derived from the simple model and the extended model for a wire counter at constant V_{ac}.

10. A comparison of the charge delivery waveforms $Q(t) / Q_0$ of the various types of gas avalanche detectors, each at their typical operating conditions.

11. Here the values of W and λ derived from the data of figures 1 and 3 (after they have been corrected for the ballistic fraction) are plotted against the reduced anode electric field in each detector. W is seen to be more sensitive to the gas composition than λ so that the points measured in argon + 7.5% methane clearly lie on a different curve (dashed) from those with 20-25% quencher.

12. A comparison of the behaviour of the gain of the wire, pin and parallel gap counters as a function of the anode dimension at constant V_{ac}, as predicted by the simple model in ambient conditions.

13. Experimental data showing the gain maximum in a GMSD counter as a function of the anode width [18]. The wire counter fit uses the approximations developed for the GMSD dimensions in section 2.2.

14. This plot shows the electric field strength at the cathode of a wire counter (r_c = 10mm) as the anode radius varies as predicted by the simple model when the gain is held constant at M = 5000.

15. The electric field strength in a parallel gap counter as the gap width varies as predicted by the simple model when the gain is held constant at M = 5000.

16. The relative sensitivity of the gain of a parallel gap counter operated at constant gain (M = 5000) to changes in the gap width (d) as a function of the gap width – as predicted by the simple model.

17. The relative sensitivity of the gain of a parallel gap counter operated at constant gain (M = 5000) to changes in the gas ambient variable (q) as a function of the gap width – as predicted by the simple model.

18. The gas gain of a GMSD detector with flowing gas measured over a period of 3 weeks, plotted as a function of q. The squares represent the gain at constant V_{ac} and the circles the gain when V_{ac} is adjusted in accord with the calibrated servo relation (55).

19. The gain data curves from a GMSD operated with a xenon + 20% CO_2 mixture at a series of hyperbaric gas pressures. (From reference [28].) Simple model fits are also shown.

20. A plot of lnM versus q at V_{ac} = 630.5V extracted from the data of figure 19 using the simple model fits to interpolate. A fit to the extended model is shown from which its parameters are deduced.

21. A comparison of the experimental gain data of figure 19 with the predictions of the extended model using the parameters obtained from figure 20.

22. A plot showing the predicted variation of the optimum wire radius in the wire counter as the gas pressure is varied over a large range. The parameters of the extended fit are derived from a fit to the data of figure 2.

23. The sequence of gain curves obtained with a GMSD as the fraction of isobutane quencher in argon is varied from 5% to 100% [18] with simple model fits.

24. The values of W and λ for the GMSD gas, as a function of the quencher fraction as derived from the simple model fits to the data of figure 23.

TABLE 1

	Gas Microstrip Detector	Cylindrical Wire Detector	Pin Array Detector	Imaging Pin Detector	Parallel Gap Detector
Reduced Anode Electric Field $X_a / 10^3$ (VK/(cm-mb))	140.0	56.4	26.0	10.9	4.52
Mean Free Path λ (μm)	0.657	0.725	1.83	3.07	4.28
Ionisation Threshold W (eV)	12.2	10.9	19.33	28.8	23.96

The values of W and λ obtained from the simple model fits for all the detector types (figures 1 and 3) shown with the corresponding anode reduced electric field.

TABLE 2

	Gas Microstrip Detector	Cylindrical Wire Detector	Pin Array Detector	Imaging Pin Detector	Parallel Gap Detector
Charge Pulse "Risetime" (τ_R)	0.103ns	1.45ns	66.4ns	0.412μs	----
Positive Ion Collection Time (τ_I)	100μs*	1.45ms	2.94ms*	11.12ms	3.92μs

The charge pulse waveform parameters τ_R and τ_I for the various types of gas detector (at their appropriate operating biases and ambient gas conditions). The asterisk indicates the ion transit time to the drift electrode; otherwise it is to the nearest cathode. The small proportion of positive ions which penetrate the grid of the parallel gap counter (≈5%) will experience a transit time of ≈5ms.

TABLE 3

	Gas Microstrip Detector	Cylindrical Wire Detector	Pin Array Detector	Imaging Pin Detector	Parallel Gap Detector
Reduced Anode Electric Field $X_a / 10^3$ (VK/(cm-mb))	140.0	56.4	26.0	10.9	4.52
Mean Free Path λ (μm)	0.672	1.06	2.06	3.07	4.28
Ionisation Threshold W (eV)	12.22	12.06	20.45	32.5	30.9

The values of W and λ obtained from the simple model fits for all the detector types (figures 1 and 3) after correction had been made to the gain data for the ballistic fraction of each detector. Also shown is the corresponding anode reduced electric field.

FIGURE 1

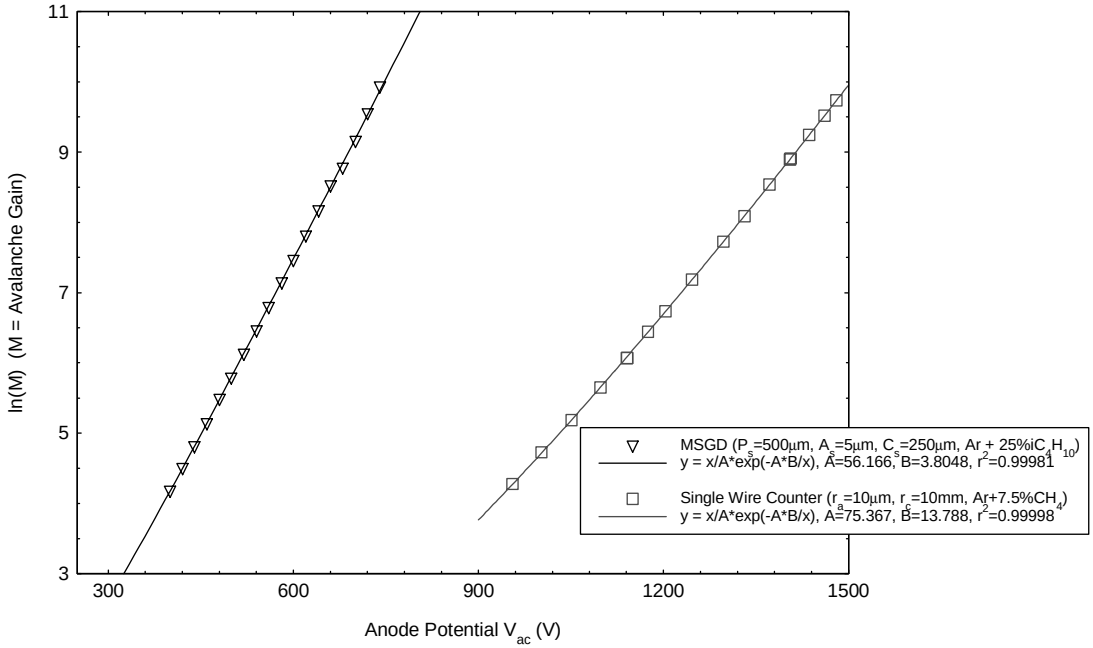

FIGURE 2

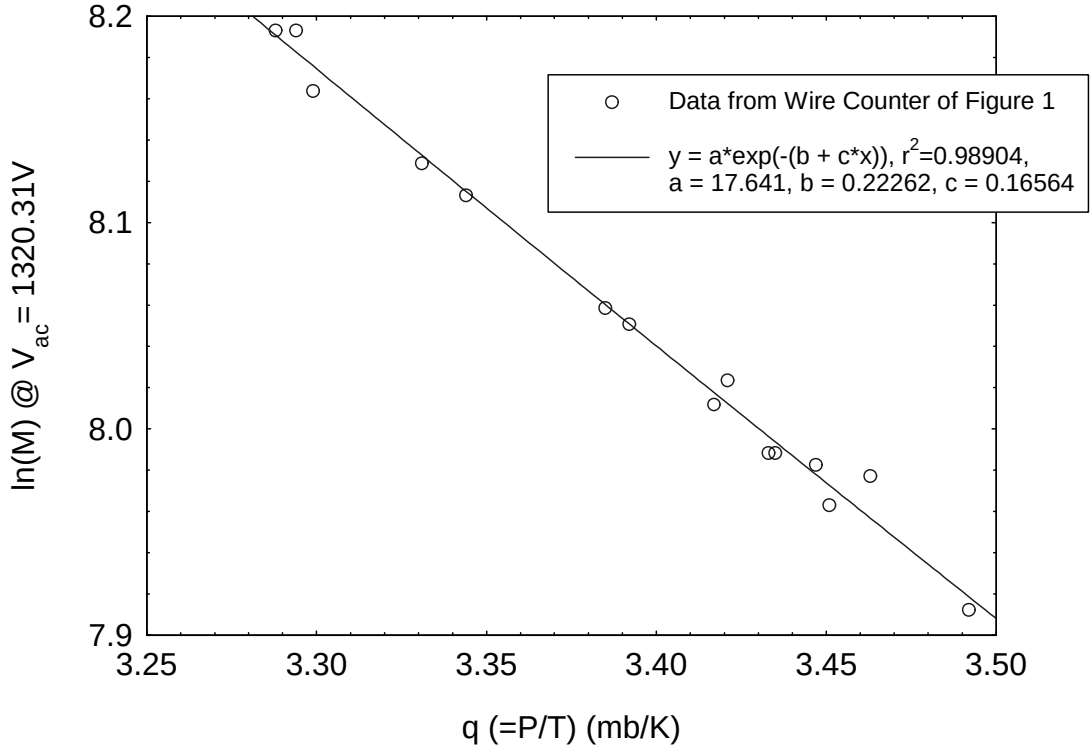

FIGURE 3

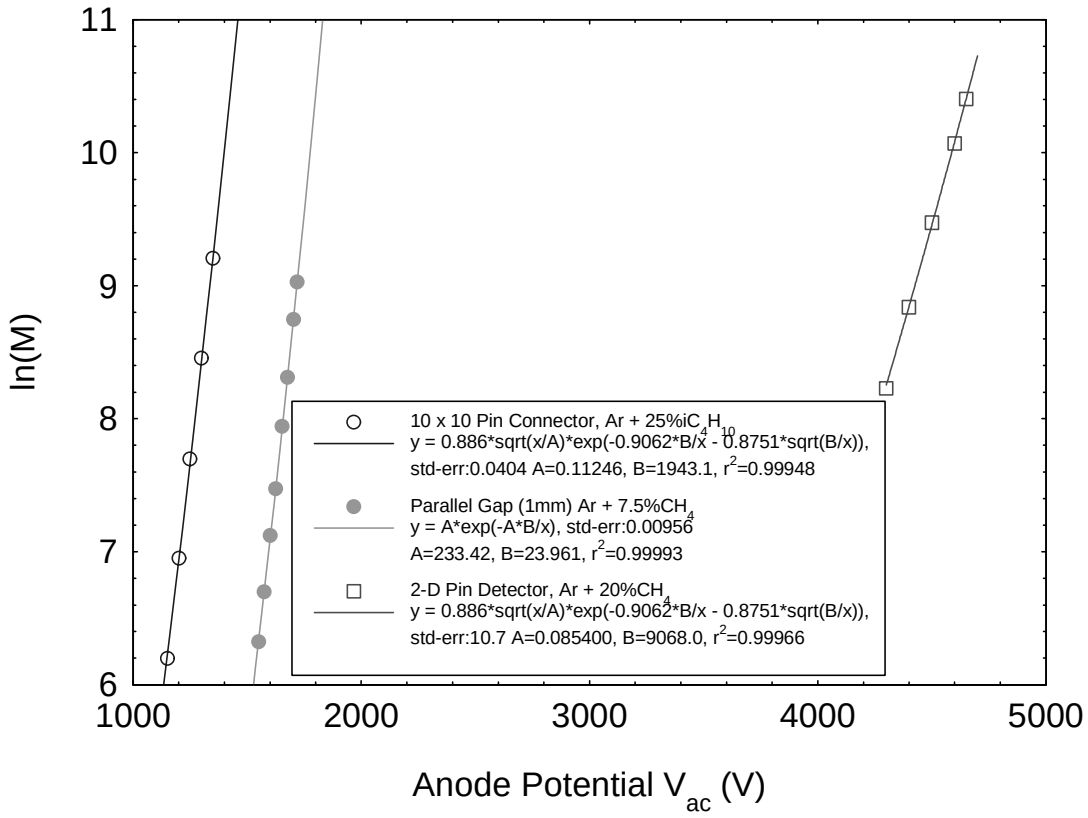

FIGURE 4

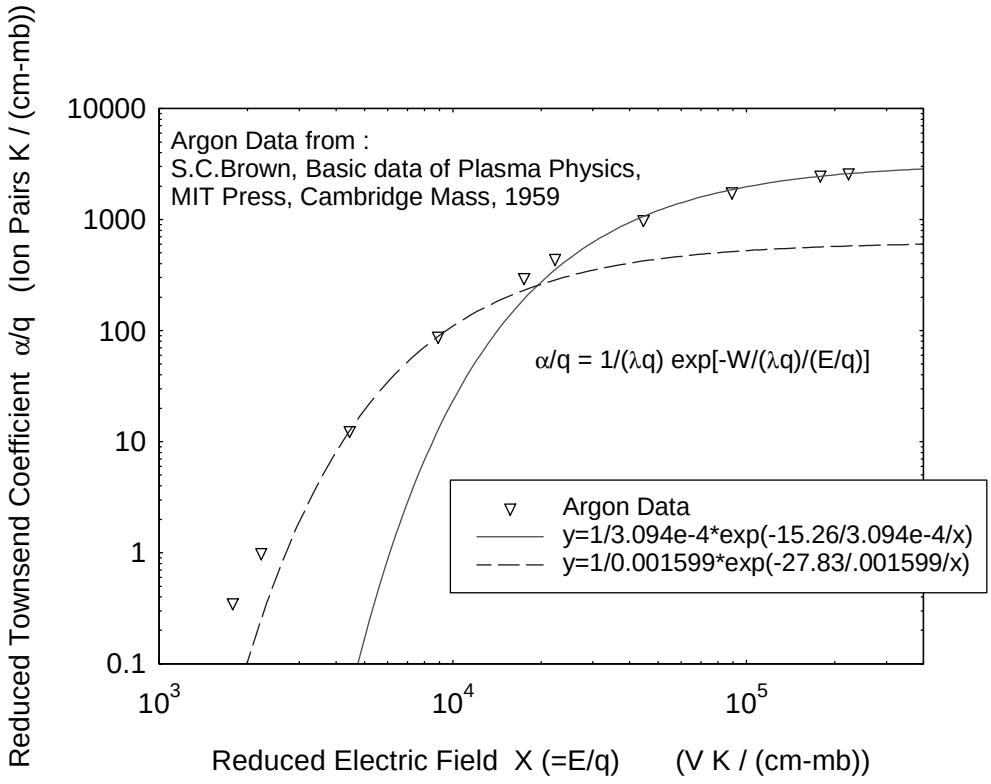

FIGURE 5

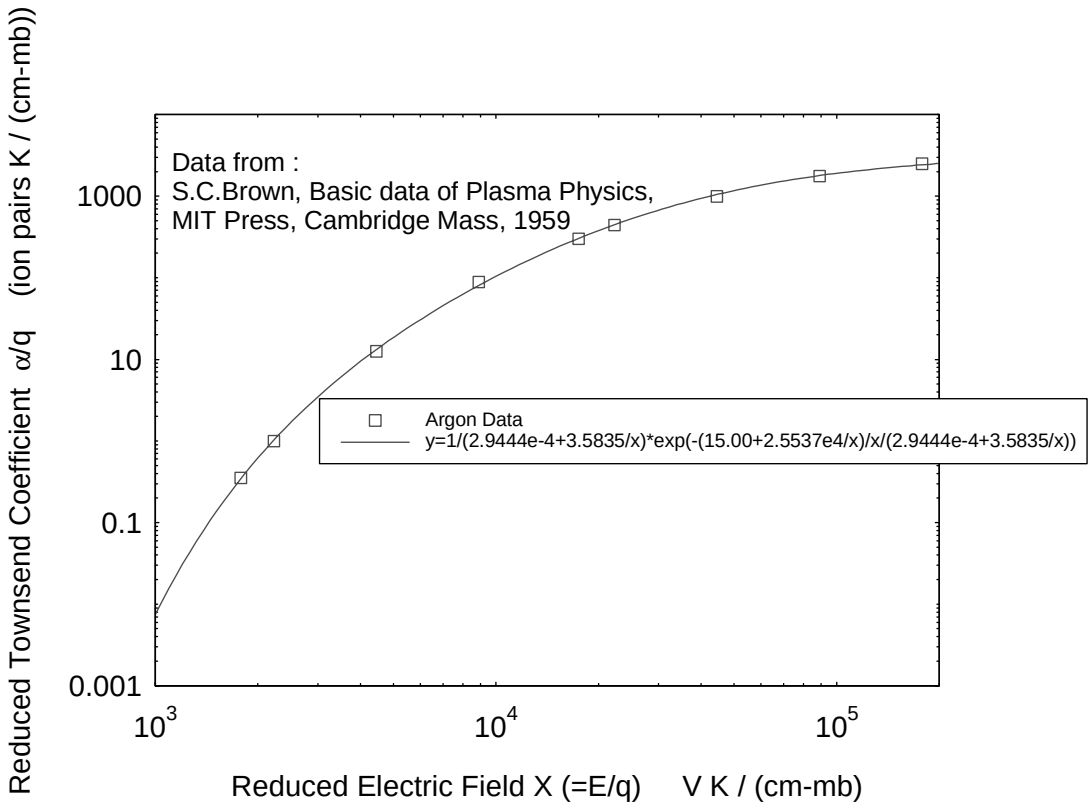

FIGURE 6

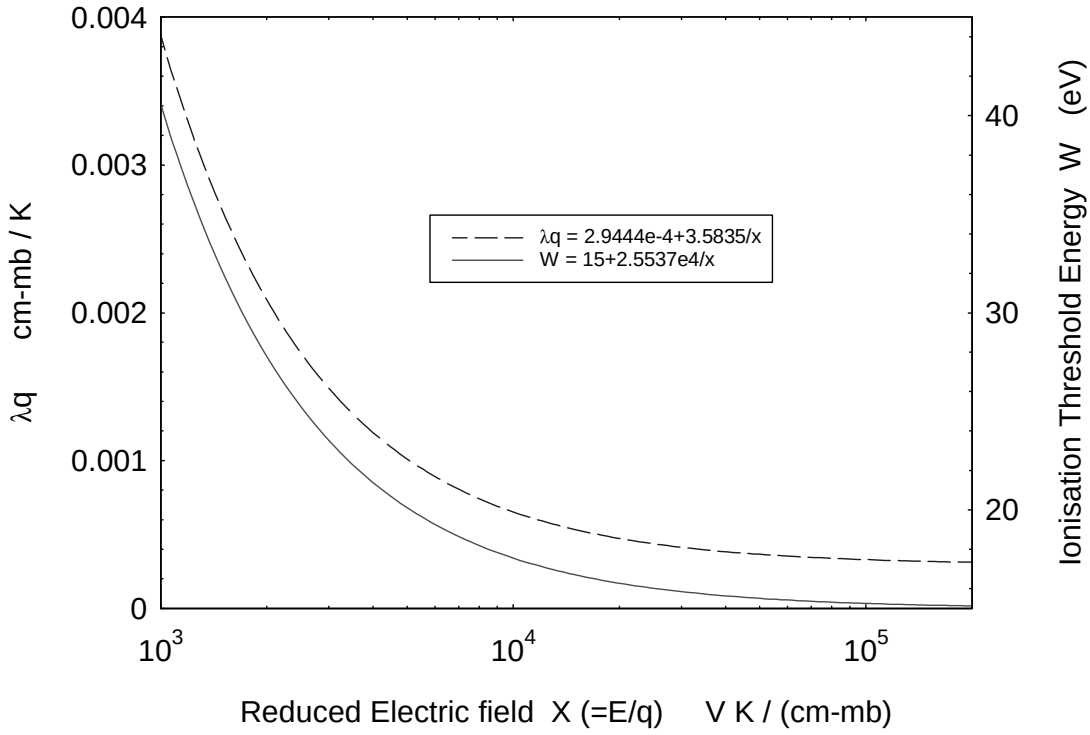

FIGURE 7

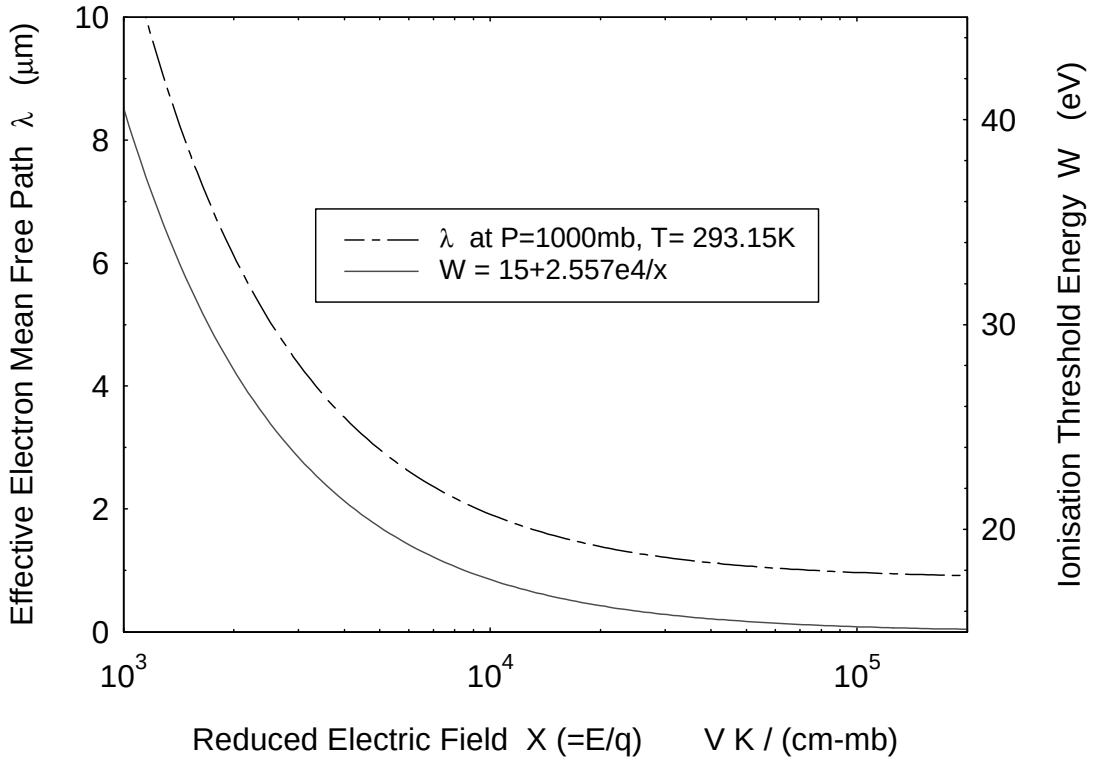

FIGURE 8

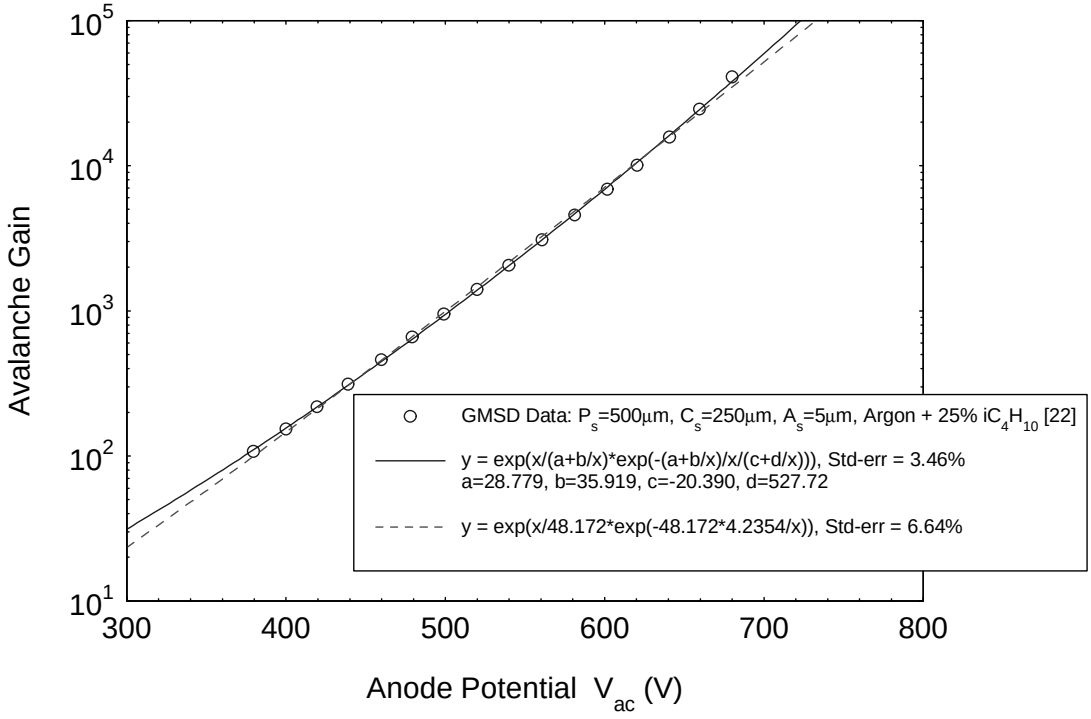

FIGURE 9

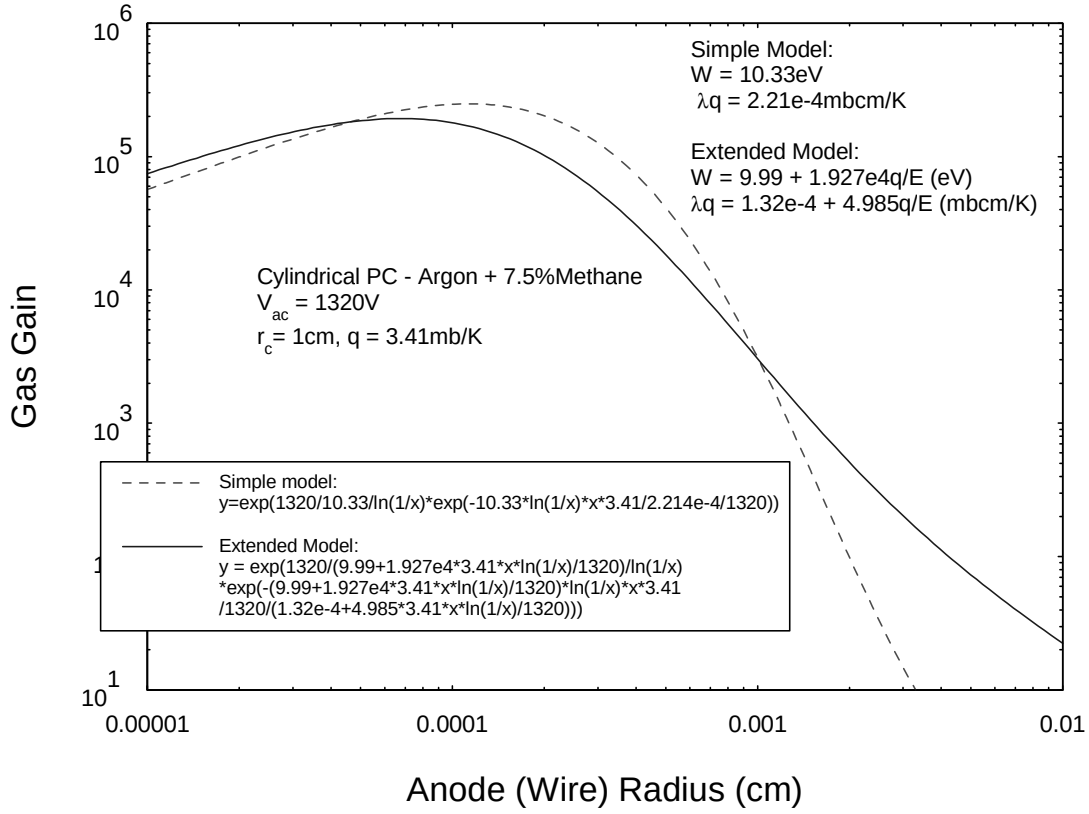

FIGURE 10

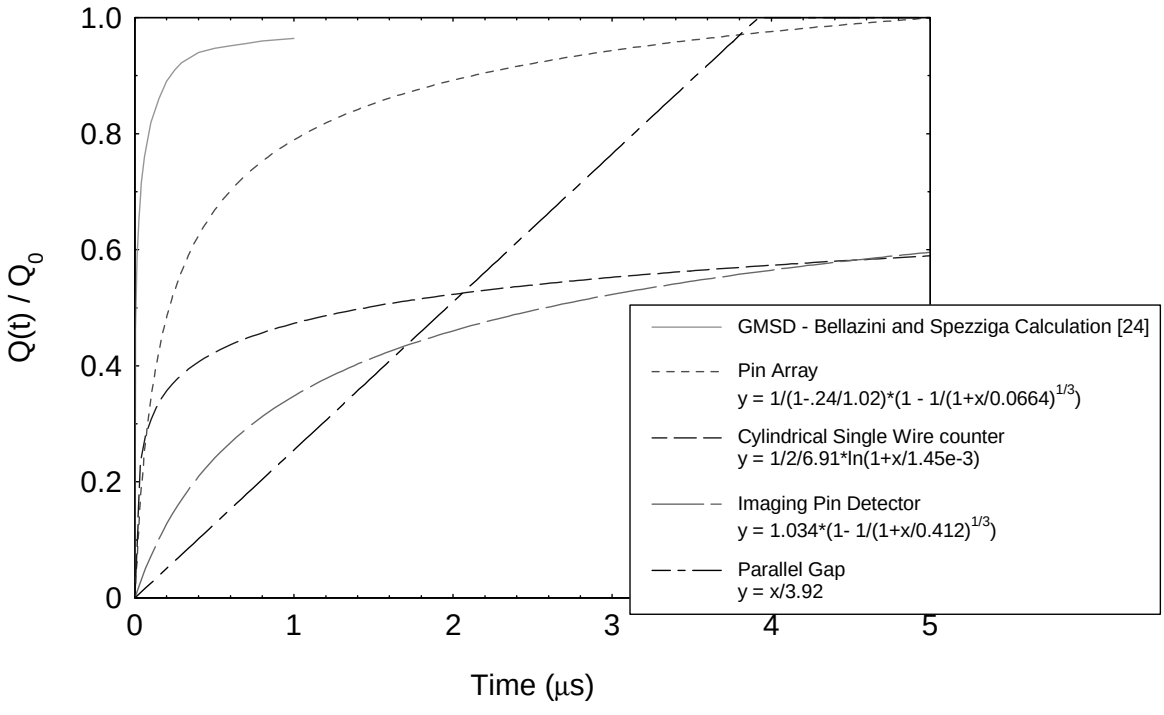

FIGURE 11

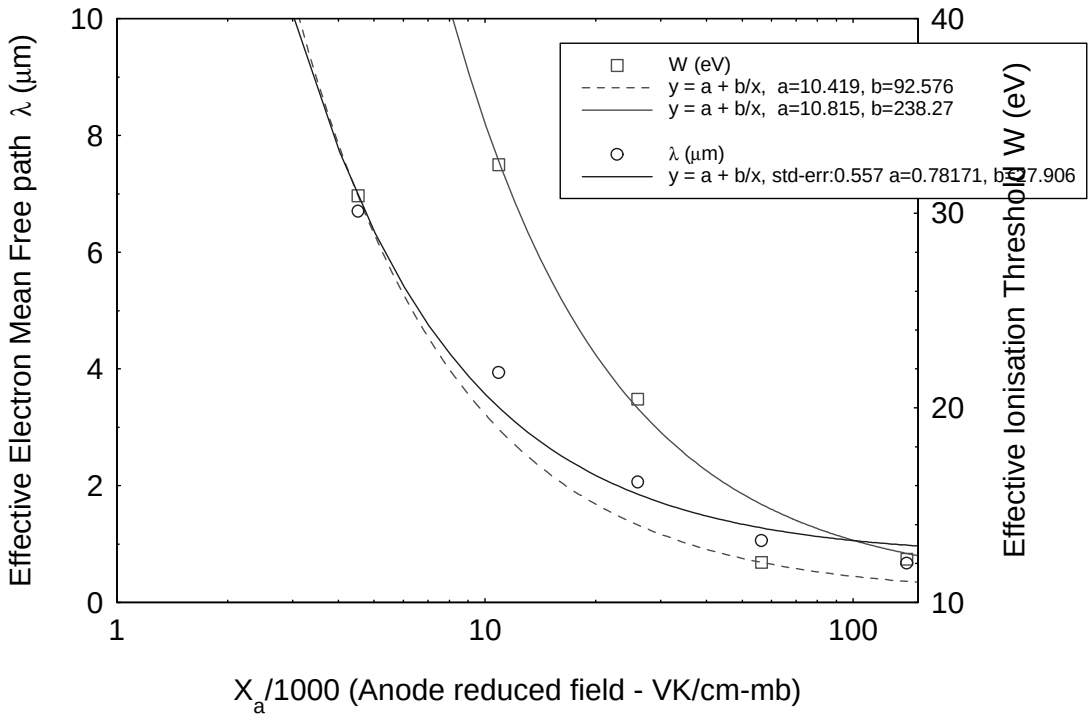

FIGURE 12

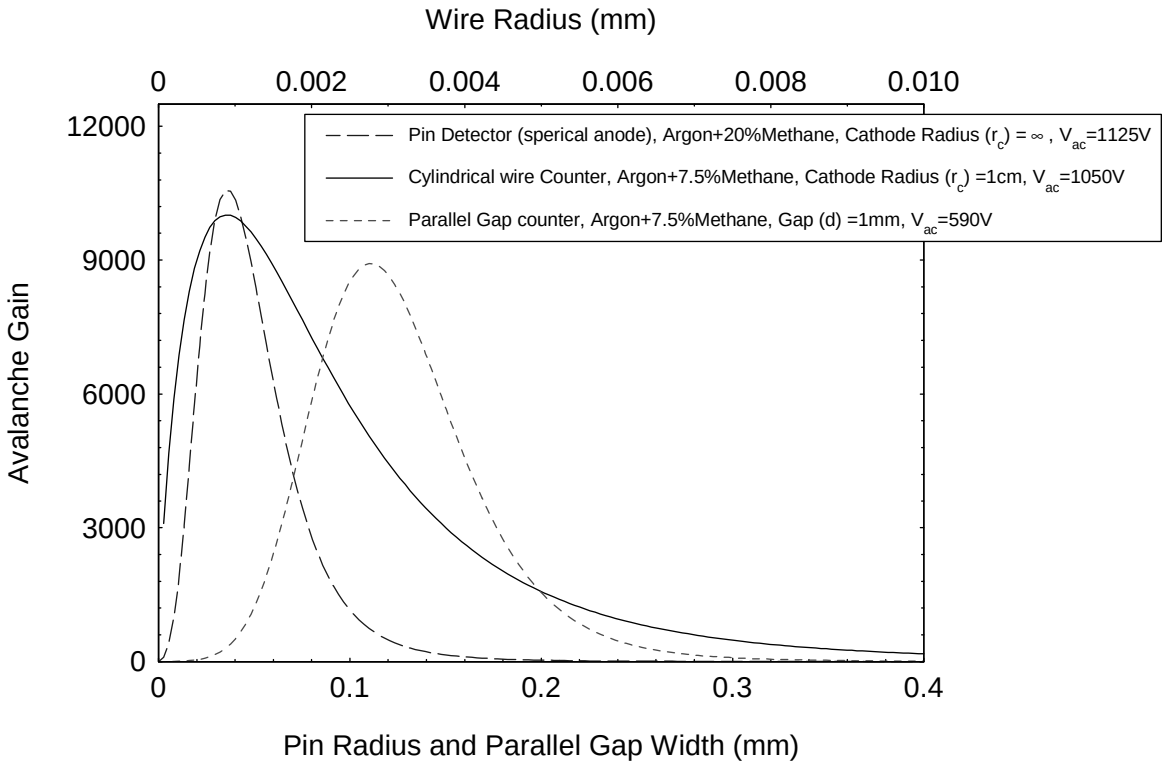

FIGURE 13

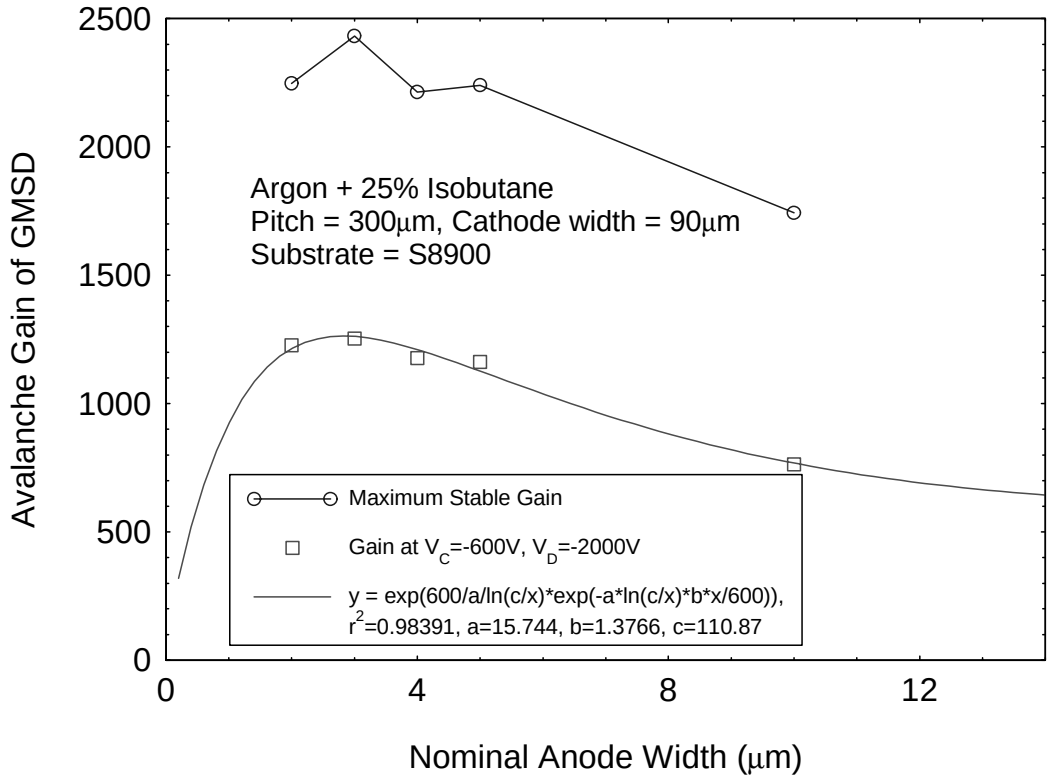

FIGURE 14

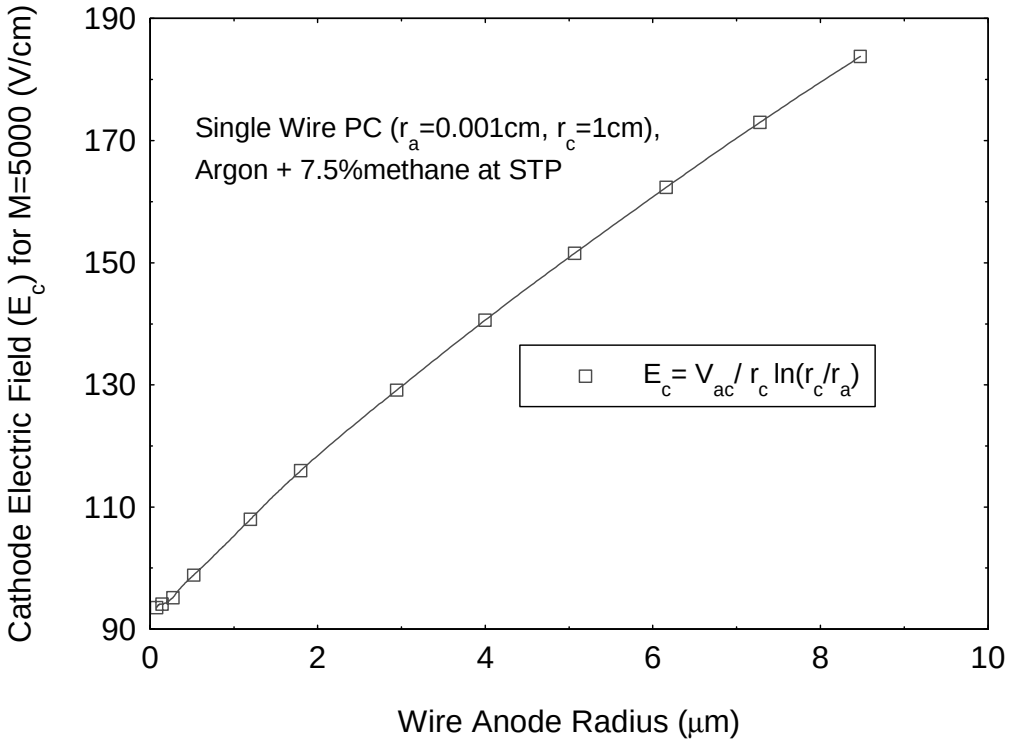

FIGURE 15

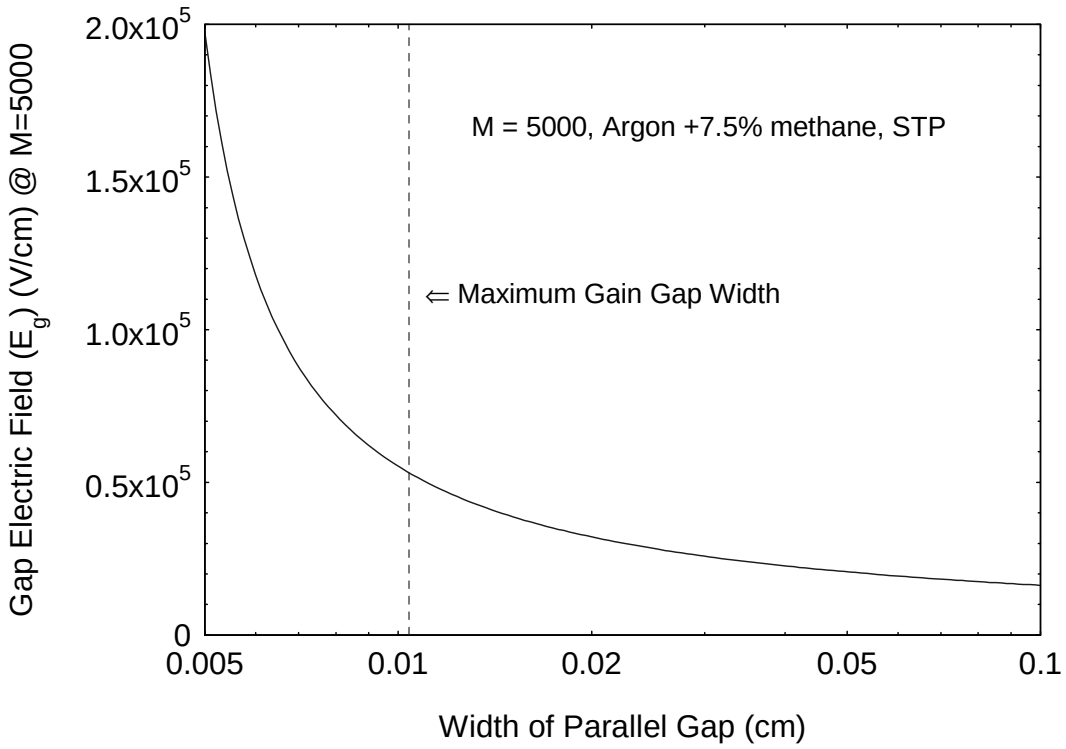

FIGURE 16

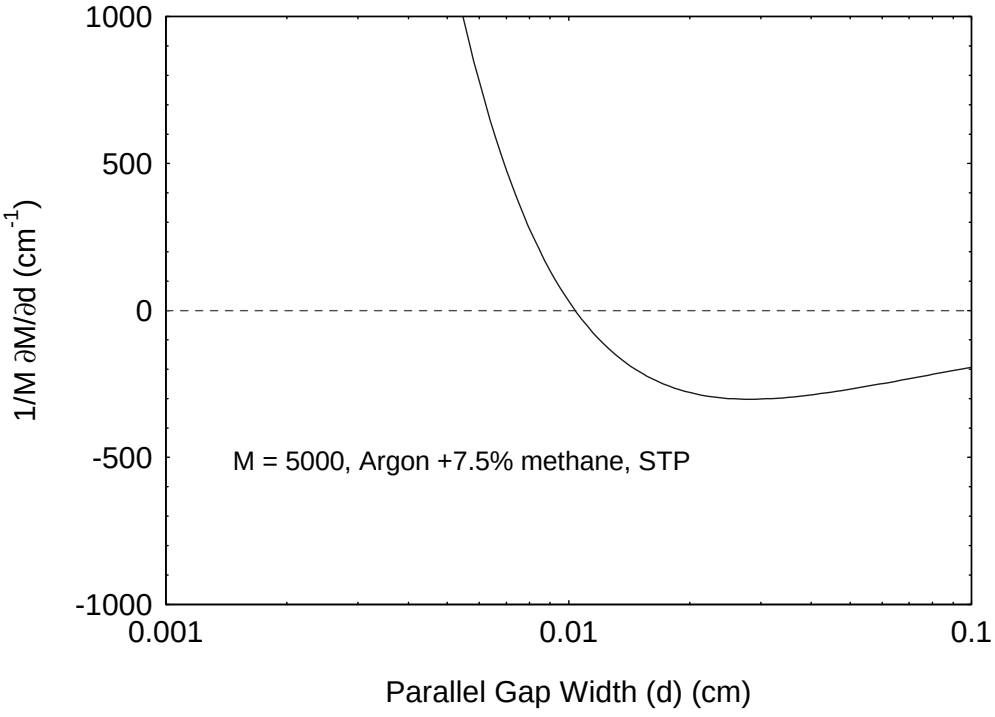

FIGURE 17

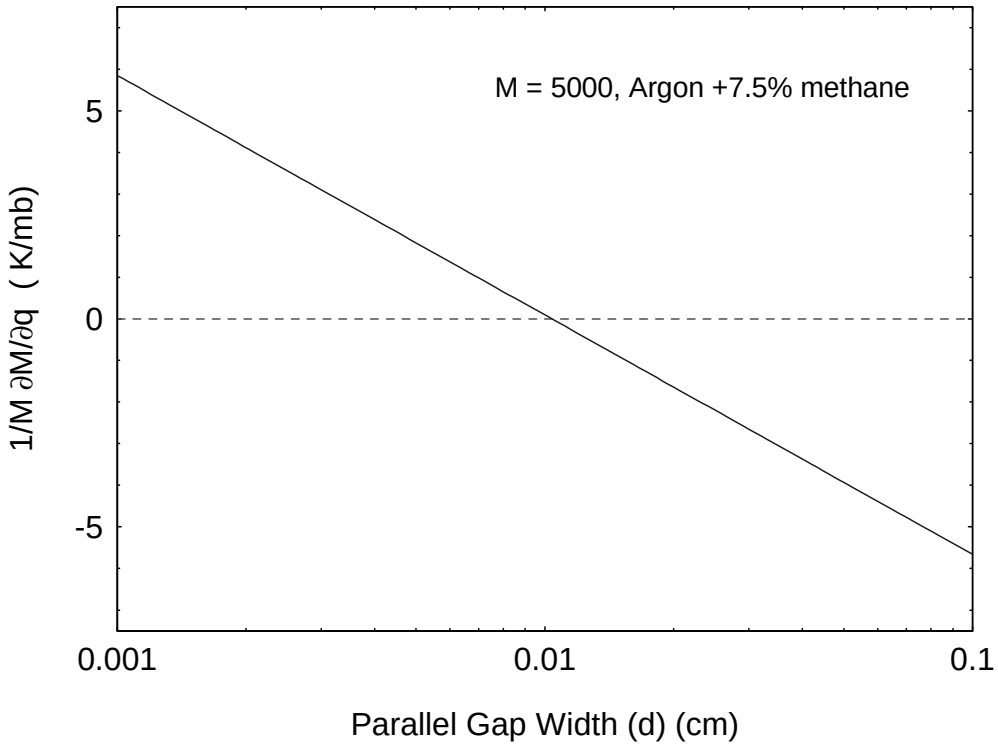

FIGURE 18

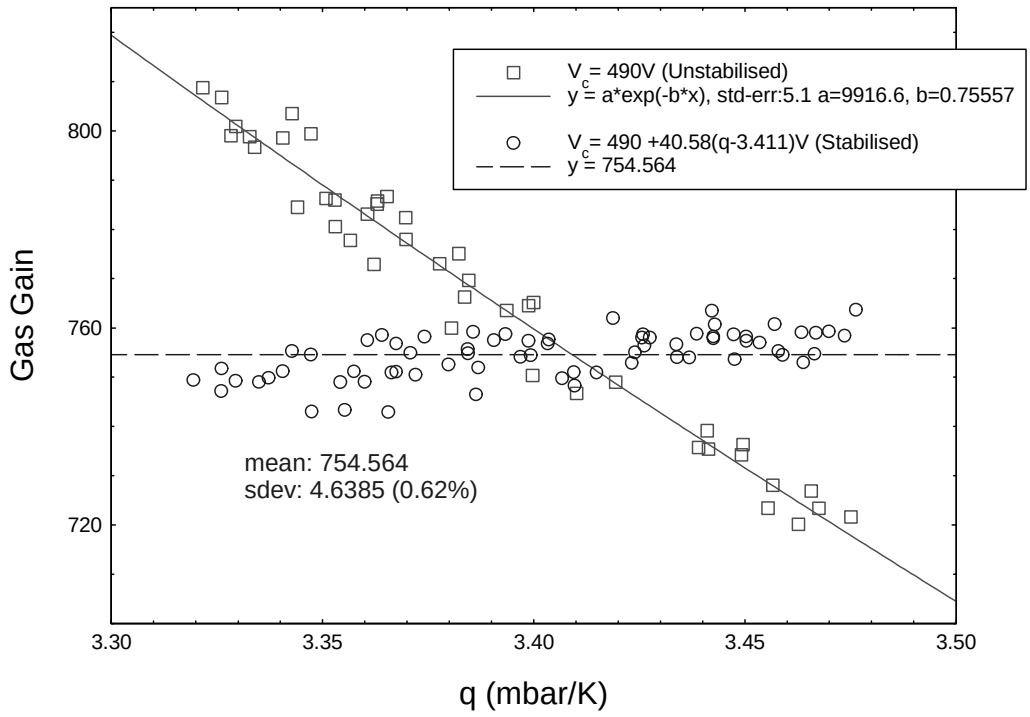

FIGURE 19

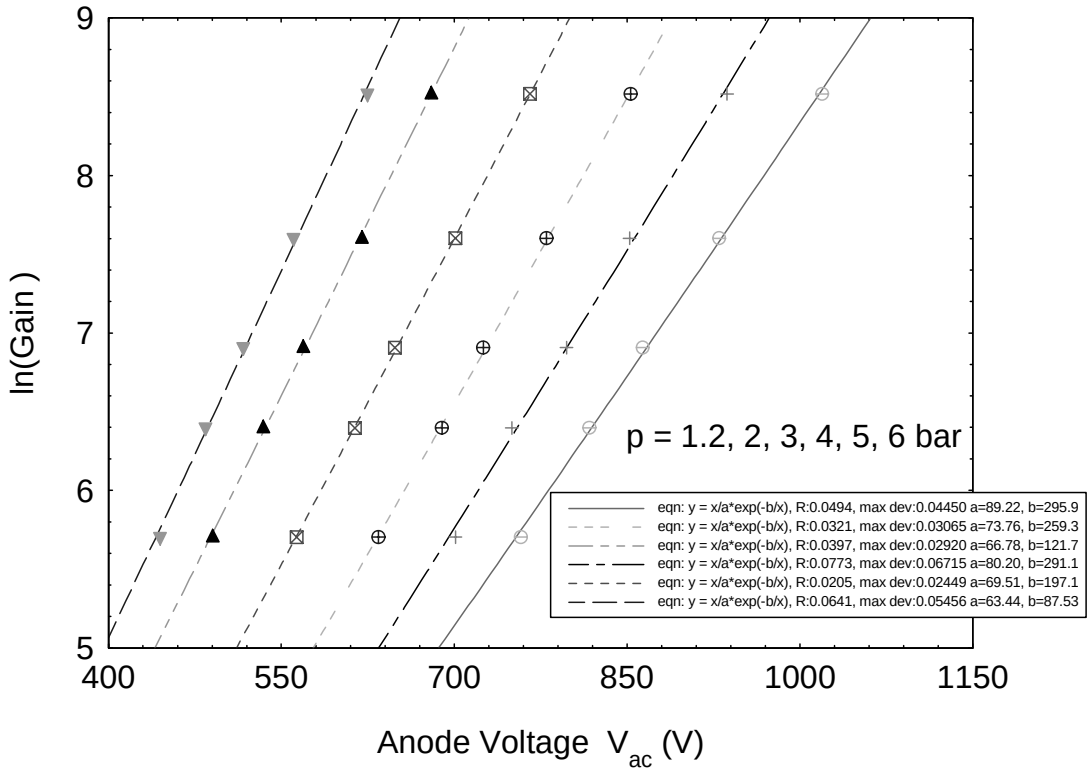

FIGURE 20

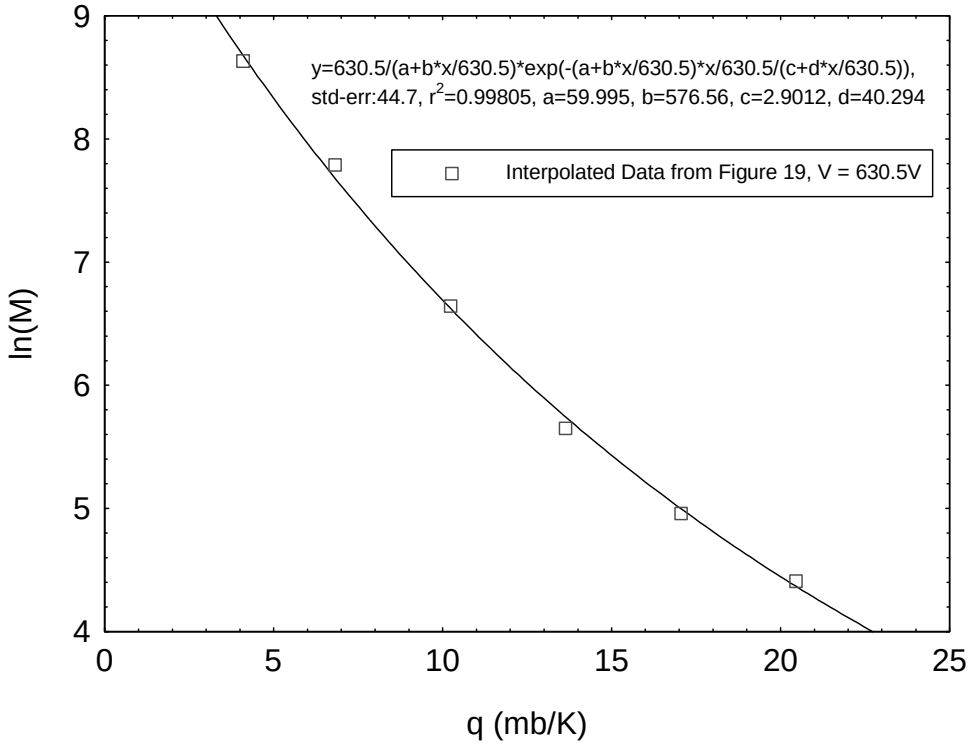

FIGURE 21

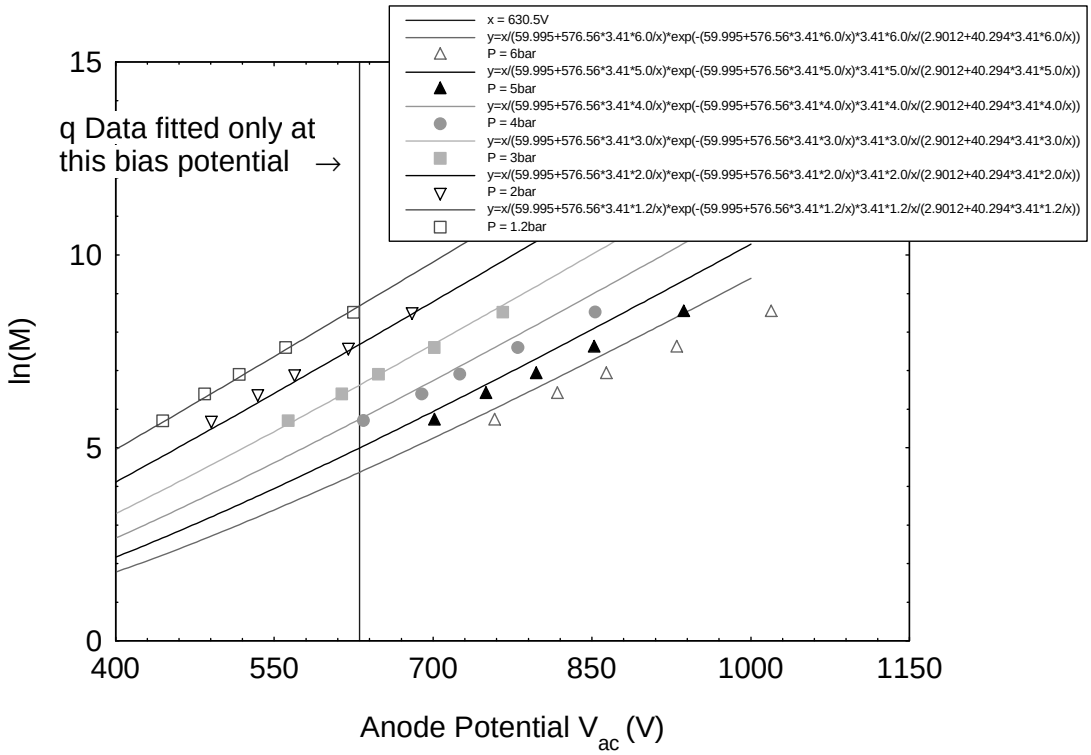

FIGURE 22

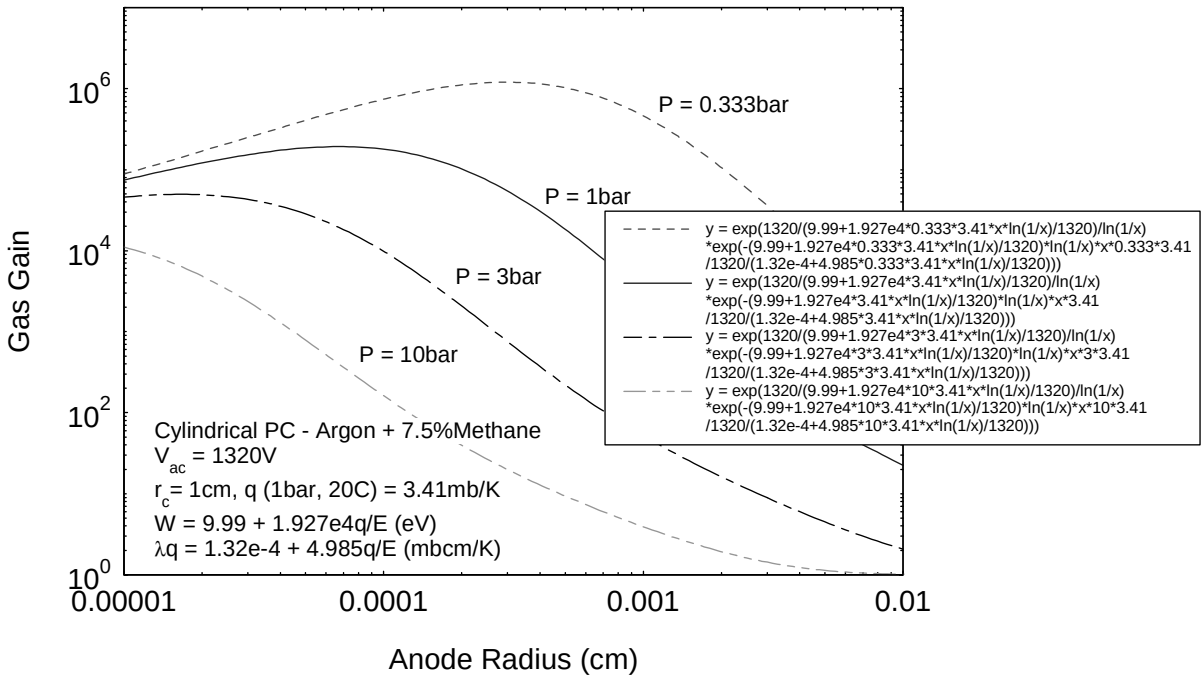

FIGURE 23

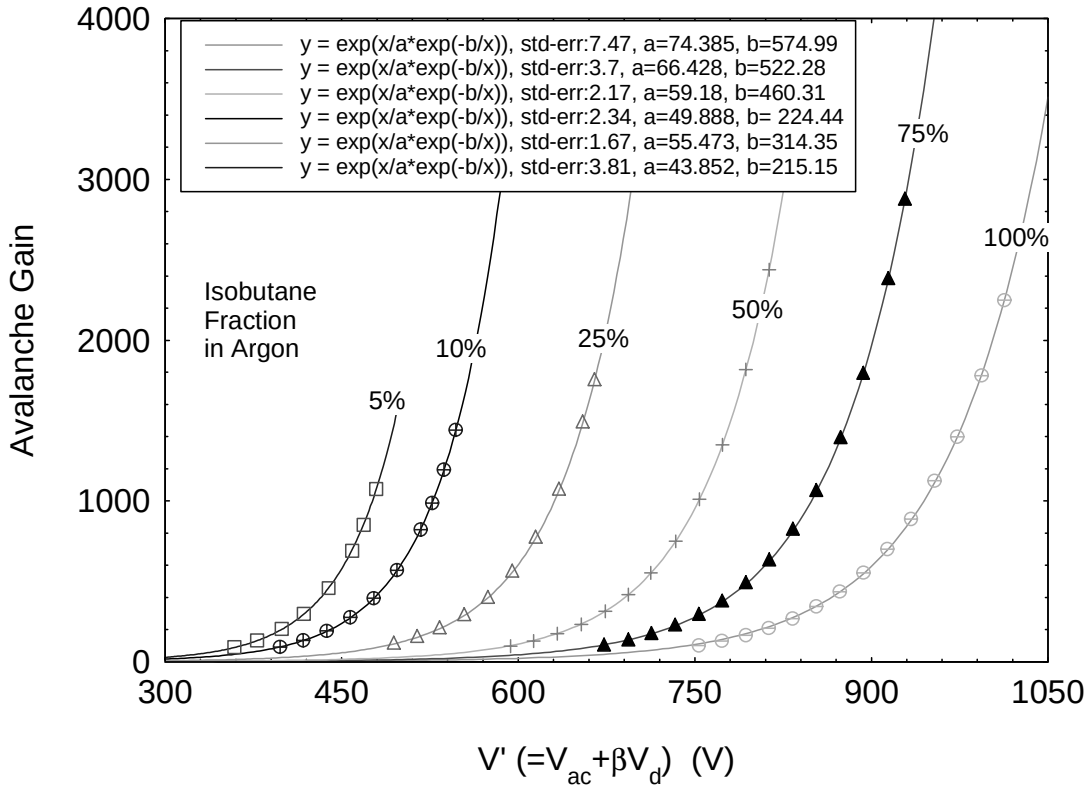

FIGURE 24